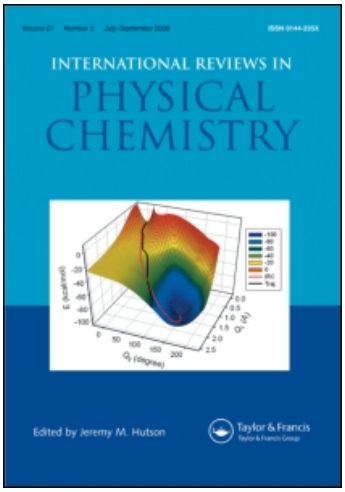

International Reviews in Physical Chemistry
Publication details, including instructions for authors and subscription information:
http://www.informaworld.com/smpp/title~content=t713724383

Spin-coupled descriptions of organic reactivity

David L. Cooper[a]; Peter B. Karadakov[b]
[a] Department of Chemistry, University of Liverpool, Liverpool, L69 7ZD, UK [b] Department of Chemistry, University of York, Heslington, York, YO10 5DD, UK

To cite this Article Cooper, David L. and Karadakov, Peter B.(2009) 'Spin-coupled descriptions of organic reactivity', International Reviews in Physical Chemistry, 28: 2, 169 — 206
To link to this Article: DOI: 10.1080/01442350902996092
URL: http://dx.doi.org/10.1080/01442350902996092

International Reviews in Physical Chemistry
Vol. 28, No. 2, April–June 2009, 169–206

Taylor & Francis
Taylor & Francis Group

Spin-coupled descriptions of organic reactivity

David L. Cooper[a]* and Peter B. Karadakov[b]*

[a]*Department of Chemistry, University of Liverpool, Liverpool, L69 7ZD, UK;*
[b]*Department of Chemistry, University of York, Heslington, York, YO10 5DD, UK*

(*Received 16 March 2009; final version received 24 April 2009*)

We survey the highly visual models of correlated electronic structure provided by spin-coupled (SC) theory for the bond-breaking and bond-formation processes along the minimum energy paths in chemical reactions. Given that SC theory uses the most general wave function based on a single orbital product, it arguably represents the highest level of theory at which one can obtain directly such orbital models. The results provide highly visual insights into the electronic rearrangements occurring in a wide range of organic chemical reactions.

Keywords: spin-coupled theory; organic reactions; modern valence bond; cycloaddition; spin functions

Contents

*Corresponding authors. Email: dlc@liverpool.ac.uk; pbk1@york.ac.uk

ISSN 0144–235X print/ISSN 1366–591X online

DOI: 10.1080/01442350902996092
http://www.informaworld.com

1. Introduction

Concepts taken from electronic structure theory have been of immense importance in the historical development of chemistry, and they continue to play a key role in the modern understanding of molecular electronic structure and reactivity. Such concepts not only allow us to rationalise but, in many cases, also to make predictions for whole classes of new systems. Classical valence bond (VB) theory played an important role in directing early qualitative models of bonding, and many VB concepts are still key components of the language of chemistry. Nonetheless, for practical calculations, VB theory has mostly been eclipsed by molecular orbital (MO) theory and, especially, density functional theory (DFT). On the other hand, several groups have shown that it is possible to develop efficient implementations of VB theory [see e.g. 1,2] that can contribute significantly to our understanding of chemical bonding and reactivity. Such VB studies also provide useful benchmarks against which popular forms of analysing MO theory and DFT electron densities can be assessed.

Simple orbital models are at the heart of the most popular and successful qualitative interpretations of electronic reaction mechanisms, such as the Woodward-Hoffmann rules [3,4], Fukui's frontier orbital theory [5], and the Dewar–Zimmerman treatment [6–8]. One common feature of these interpretations is that they are all based on rather low-level semi-empirical quantum-chemical approaches, such as Hückel molecular orbital (HMO) theory or its extended version (EHT). The many-electron wave function in HMO and EHT is a single Slater determinant, in which the orbitals can be only doubly or singly-occupied. As a rule, the qualitative features of the HMO and EHT orbitals do not change much at higher levels of theory, if the wave function remains a single Slater determinant, and are usually well-reproduced by *ab initio* Hartree–Fock calculations. However, it is now widely acknowledged that the accurate description of the potential energy surface for a reacting system requires a significantly more advanced *ab initio* wave function constructed at or beyond the complete active space self-consistent field (CASSCF) level of theory. A wave function of this type typically involves a large number of configurations. If the wave function is dominated by a very small number of configurations, or if all active space orbitals have occupation numbers very close to one or two, then it is still possible to think that the shapes of the active space orbitals carry some qualitative electronic structure information. However, in many cases all configurations have relatively small weights and a number of active space orbitals have distinctly fractional occupation numbers; while numerically accurate, a wave function with these characteristics is probably too complicated to allow a meaningful direct interpretation in qualitative terms. As spin-coupled (SC) theory uses the most general wave function based on a single orbital product, it arguably represents the highest level of theory at which one can obtain directly orbital models of the bond-breaking and bond-formation processes accompanying organic chemical reactions.

2. The SC wave function

Spin-coupled theory makes use of the most general N-electron wave function based on a single orbital product which can be written (in unnormalised form) as

$$\Psi_{SM} = \hat{A}(\psi_1\psi_2 \ldots \psi_N\Theta^N_{SM}) \tag{1}$$

In this expression $\hat{A}$ stands for the antisymmetriser, ψ_1–ψ_N are singly-occupied orbitals, free from any orthogonality restrictions (often referred to as spin-coupled orbitals) and Θ^N_{SM} is a general N-electron spin eigenfunction which can be expanded in a suitable N-electron spin basis

$$\Theta^N_{SM} = \sum_{k=1}^{f^N_S} C_{Sk}\Theta^N_{SM;k} \tag{2}$$

The subscripts S and M indicate that $\Theta^N_{SM;k}$ is a simultaneous eigenfunction of the operators for the total spin of the system $\hat{S}^2$ and its z-projection $\hat{S}_z$, with eigenvalues $S(S+1)$ and M, respectively, in atomic units. The index k distinguishes between the f^N_S unique spin eigenfunctions sharing the same pair of S and M values:

$$f^N_S = \binom{N}{N/2-S} - \binom{N}{N/2-S-1} \tag{3}$$

The orbitals ψ_1–ψ_N are approximated by MO-style expansions within a suitable atomic orbital (AO) basis $\{\chi_p | p = 1, 2, \ldots, m\}$

$$\psi_\mu = \sum_{p=1}^{m} c_{\mu p}\chi_p \tag{4}$$

Equations (1) and (2) define the SC wave function proposed by Gerratt and Lipscomb [9]. An identical wave function *ansatz* was introduced slightly later by Ladner and Goddard [10], with the appellation full generalised valence bond (full-GVB) wave function.

The optimal SC orbitals [Equation (4)] and spin-coupling pattern [Equation (2)] are determined variationally, through a simultaneous optimisation of the energy expectation value corresponding to the SC wave function in Equation (1) [11,12]

$$E = \frac{\langle\Psi_{SM}|\hat{H}|\Psi_{SM}\rangle}{\langle\Psi_{SM}|\Psi_{SM}\rangle} = D^{-1}\left[\sum_{\mu,\nu=1}^{N} D(\mu|\nu)\langle\mu|\hat{h}|\nu\rangle + \frac{1}{2}\sum_{\mu,\nu,\sigma,\tau=1}^{N} D(\mu\nu|\sigma\tau)\langle\mu\nu|\sigma\tau\rangle\right] \tag{5}$$

with respect to all orbital and spin-coupling coefficients $c_{\mu p}$ and C_{Sk}. In this equation, $\hat{H}$ denotes the standard non-relativistic electronic Hamiltonian

$$\hat{H} = \sum_{i=1}^{N}\hat{h}_i + \tfrac{1}{2}\sum_{i\neq j}^{N} r_{ij}^{-1} \tag{6}$$

where $\langle\mu\nu|\sigma\tau\rangle = \langle\mu(1)\nu(2)|r_{12}^{-1}|\sigma(1)\tau(2)\rangle$ are two-electron integrals over SC orbitals, while D, $D(\mu|\nu)$ and $D(\mu\nu|\sigma\tau)$ stand for the SC normalisation integral (zeroth-order density matrix), and the elements of the SC first- and second-order spinless density matrices, respectively.

At first glance, there is no immediate reason to classify the SC wave function Ψ_{SM} in Equation (1) as a VB, rather than as a MO theory construction. In fact, Ψ_{SM} can be viewed as a generalisation of a group of approaches, which have always been thought of as MO-based: the closed-shell, open-shell and spin-projected Hartree–Fock methods. The link between the SC approach and classical VB theory is revealed by an alternative

representation of the SC wave function [Equation (1)] as a combination of (or, more succinctly, resonance between) f_S^N VB-style structures

$$\Psi_{SM} = \sum_{k=1}^{f_S^N} C_{Sk} \Psi_{SM;k} \tag{7}$$

where

$$\Psi_{SM;k} = \hat{A}(\psi_1 \psi_2 \ldots \psi_N \Theta_{SM;k}^N) \tag{8}$$

The resonance energy relative to any structure $\Psi_{SM;k}$ can be taken to be equal to the difference between its energy expectation value and the full SC energy.

Although the expansion in terms of resonance structures in Equation (7) is valid for any set of spin eigenfunctions, the link to VB theory is most apparent when use is made of the Rumer spin basis. In the case of well-localised SC orbitals, it becomes possible to establish a direct analogy with the covalent structures of classical VB theory.

In MO theory, the expansion in Equation (7) would be regarded as a multi-configuration (MC) construction in terms of configurations state functions (CSFs), which include the same product of non-orthogonal orbitals in combination with different spin functions [Equation (8)].

The calculation of SC wave functions requires significant computational effort which arises mainly from the use of non-orthogonal orbitals and of the full spin space. This restricts the number of SC orbitals that can be handled by existing codes on current computer systems to about 14. However, sufficiently accurate descriptions of many chemical problems can be achieved by applying a higher-level approach to a limited subset of 'active' (or 'valence') orbitals only, while keeping the remaining 'inactive' (or 'core') orbitals doubly-occupied. Typical examples of orbitals that can be left doubly-occupied are given by the orbitals making up the inner shells of atoms and by the σ orbitals in π electron treatments of planar conjugated molecules. The introduction of core–valence separation leads to a significant reduction of the numerical effort required for computing any post-Hartree–Fock wave function and allows calculations on systems with much larger numbers of electrons. The idea was first suggested by McWeeny [13] in the context of an orthogonalised VB approach. Its implementation within any post-Hartree–Fock method, including SC theory, is reasonably straightforward.

The introduction of n doubly-occupied core orbitals changes the expression defining the SC wave function [Equation (1)] to (for further details, see [14])

$$\Psi_{SM} = \hat{A}(\overbrace{\varphi_1^2 \varphi_2^2 \ldots \varphi_n^2 \underbrace{\alpha\beta\alpha\beta \ldots \alpha\beta}_{n\ \alpha\beta\ \text{pairs}}}^{\text{core}} \psi_1 \psi_2 \ldots \psi_N \Theta_{SM}^N) \tag{9}$$

It can be shown that this wave function is invariant (except for the multiplication by a constant factor) to any non-singular linear transformation mixing the n core orbitals, and does not change if a multiple of any core orbital is added to any valence orbital. As a consequence, without any loss of generality, the set of core orbitals can be taken to be orthonormal and orthogonal to the valence orbitals. Due to these orthogonality

properties, the expression for the electronic energy of wave function (9) can be written down in a form which closely resembles Equation (5)

$$E = E_c + D^{-1}\left[\sum_{\mu,\nu=1}^{N} D(\mu|\nu)\langle\mu|\hat{f}_c|\nu\rangle + \frac{1}{2}\sum_{\mu,\nu,\sigma,\tau=1}^{N} D(\mu\nu|\sigma\tau)\langle\mu\nu|\sigma\tau\rangle\right] \tag{10}$$

The term E_c corresponds to the core energy

$$E_c = \sum_{i=1}^{n}\langle i|\hat{h} + \hat{f}_c|i\rangle \tag{11}$$

and $\hat{f}_c$ stands for the Fock operator for the core orbitals, which involves the well-known Coulomb and exchange operators $\hat{J}_i$ and $\hat{K}_i$ associated with core orbital φ_i

$$\hat{f}_c = \hat{h} + \sum_{i=1}^{n}(2\hat{J}_i - \hat{K}_i) \tag{12}$$

The core orbitals are expanded in the same basis as the SC orbitals [*cf.* Equation (4)],

$$\varphi_i = \sum_{p=1}^{m} c_{ip}\chi_p \tag{13}$$

The most significant computational savings associated with the introduction of the core–valence separation are achieved when the core orbitals are kept fixed, which reduces the computational effort required for a calculation on a system with $2n+N$ electrons to that for a system with N electrons. The simultaneous optimisation of all core and valence orbitals and spin-coupling coefficients is more expensive computationally, but not prohibitively so, even if use is made of the second-order constrained optimisation procedure described in [14]; newer approaches based on the CASVB strategy [15–19] are usually considerably faster.[1]

The use of different types of spin functions to construct the N-electron spin eigenfunction Θ^N_{SM} [Equation (2)] can highlight particular aspects of the optimal spin-coupling pattern established between the SC orbitals. Most applications of SC theory make use of the sets of spin functions introduced by Rumer [20], Kotani [21] and Serber [22,23]. These three sets of spin functions are constructed using *synthetic* methods. The full N-electron spin basis is assembled consecutively from smaller units, starting with a one- or two-electron spin function and adding a single one- or two-electron spin function at a time. In an alternative *analytic* method, introduced by Löwdin [24,25], the spin eigenfunctions are obtained by projecting out the components with the required S value from a suitable set of f^N_S linearly independent products of N one-electron spin functions with the same $M = S$ value (this corresponds to the so-called *principal case*, which is assumed throughout this article; spin functions corresponding to other values of M can be obtained by application of appropriate step-up and step-down operators).

Each of the f^N_S unique spin functions within the Rumer spin basis represents a product of $N_\beta = \frac{1}{2}N - S$ singlet pairs and $2S$ α spin functions

$$\begin{aligned}{}^{R}\Theta^N_{SM;k} = {} & \frac{1}{\sqrt{2}}[\alpha(\mu_1)\beta(\mu_2) - \alpha(\mu_2)\beta(\mu_1)]\ldots\frac{1}{\sqrt{2}}[\alpha(\mu_{N-2S-1})\beta(\mu_{N-2S}) \\ & - \alpha(\mu_{N-2S})\beta(\mu_{N-2S-1})]\alpha(\mu_{N-2S+1})\ldots\alpha(\mu_N)\end{aligned} \tag{14}$$

A spin function of this type is fully identified by the list of its singlet pairs

$$k \equiv (\mu_1 - \mu_2, \mu_3 - \mu_4, \ldots, \mu_{N-2S-1} - \mu_{N-2S}) \tag{15}$$

In fact, the number of spin functions that can be formed according to Equation (14)

$$v_S^N = \frac{N!}{2^{N_\beta}(N-2N_\beta)!N_\beta!} \tag{16}$$

is significantly larger than f_S^N which indicates that some of these are linearly dependent. The diagrammatic technique suggested by Rumer [20] and extended to non-singlet states by Simonetta *et al*. [26] offers one way of selecting f_S^N unique functions $\Theta_{SM;k}^N$. In this approach, each Rumer spin eigenfunction is derived from an extended Rumer diagram. The diagrams for a system with N electrons and spin quantum number S are based on convex (usually regular) polygons with $N+1$ vertices. The first N vertices are labelled, say clockwise, with the numbers from 1 to N, and the last vertex becomes the pole (P). Then $\frac{1}{2}N-S$ lines are drawn between pairs of the first N vertices and additional lines are drawn between the remaining $2S$ points and the pole; none of these lines are allowed to intersect. It can be shown [26] that the number of distinct extended Rumer diagrams which can be drawn in this way is f_S^N, and the associated Rumer spin eigenfunctions, in which the singlet pairs contain electrons with numbers connected by the first $\frac{1}{2}N-S$ lines, while the remaining electrons (with numbers connected to the pole) are placed within α spin functions are linearly independent. All extended Rumer diagrams and the corresponding Rumer spin functions for $N=5$ and $S=½$ ($f_{1/2}^5 = 5$) are shown in Figure 1.

Another option is to make use of the *leading term* algorithm [26] which is particularly suitable for computer implementations. Each leading term represents an ordered product of $N_\alpha = (\frac{1}{2}N+S)$ α spin functions and$N_\beta = (\frac{1}{2}N-S)$ β spin functions. The first leading term can be written as

$$\underbrace{\alpha\beta\alpha\beta\ldots\alpha\beta}_{\substack{N_\beta \\ \alpha\beta \text{ pairs}}}\ \underbrace{\alpha\alpha\ldots\alpha}_{\substack{N_\alpha-N_\beta \\ \alpha \text{ functions}}} \tag{17}$$

and each of the following leading terms $(2, 3, \ldots, f_S^N)$ is obtained from the previous one by shifting one place to the right the first β (reading from left to right) that is followed by an α, after which all β functions to the left of the one that was shifted are returned

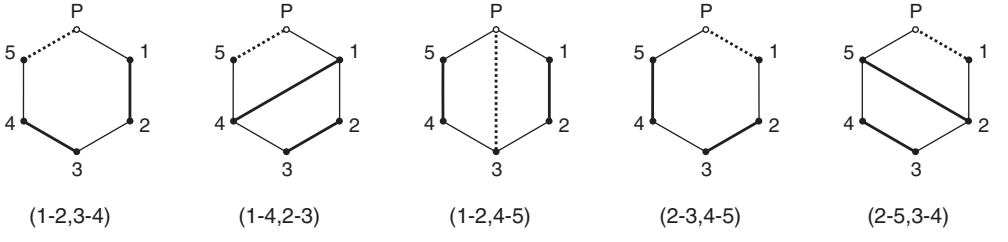

Figure 1. Extended Rumer diagrams and Rumer spin functions for $N=5$ and $S=½$.

to the positions they used to occupy in the first leading term. Then each leading term is converted into a Rumer function by inserting a left parenthesis in front of each α, and a right parenthesis after each β (again reading from left to right); every combination of α and β functions enclosed in matching left and right parentheses gives rise to a singlet pair. The following example shows the sequence of leading terms and the associated Rumer spin functions for $N=5$ and $S=½$

$$
\begin{array}{llll}
\underbrace{\alpha\beta\alpha\beta\alpha}_{\text{leading term 1}} & & \longrightarrow (\alpha\beta)(\alpha\beta)(\alpha) & = \underbrace{(1-2,3-4)}_{\text{Rumer function 1}} \\
\underset{\text{shift}}{\alpha\beta\alpha\beta\alpha} \longrightarrow \underbrace{\alpha\alpha\beta\beta\alpha}_{\text{leading term 2}} & & \longrightarrow (\alpha(\alpha\beta)\beta)(\alpha) & = \underbrace{(1-4,2-3)}_{\text{Rumer function 2}} \\
\underset{\text{shift}}{\alpha\alpha\beta\beta\alpha} \longrightarrow \underset{\text{return}}{\alpha\alpha\beta\alpha\beta} \longrightarrow \underbrace{\alpha\beta\alpha\alpha\beta}_{\text{leading term 3}} & & \longrightarrow (\alpha\beta)(\alpha(\alpha\beta)) & = \underbrace{(1-2,4-5)}_{\text{Rumer function 3}} \\
\underset{\text{shift}}{\alpha\beta\alpha\alpha\beta} \longrightarrow \underbrace{\alpha\alpha\beta\alpha\beta}_{\text{leading term 4}} & & \longrightarrow (\alpha(\alpha\beta)(\alpha\beta)) & = \underbrace{(2-3,4-5)}_{\text{Rumer function 4}} \\
\underset{\text{shift}}{\alpha\alpha\beta\alpha\beta} \longrightarrow \underbrace{\alpha\alpha\alpha\beta\beta}_{\text{leading term 5}} & & \longrightarrow (\alpha(\alpha(\alpha\beta)\beta)) & = \underbrace{(2-5,3-4)}_{\text{Rumer function 5}}
\end{array}
\tag{18}
$$

The Kotani spin functions ${}^{\mathrm{K}}\Theta^{N}_{SM;k}$ are formed through successive coupling of individual electron spins according to the rules for addition of angular momenta. A Kotani spin function is completely defined by the sequence of partial resultant spins obtained after combining the spins of the first $1, 2, \ldots, N-1$ electrons, which can be used as a convenient shorthand representation of the spin function (there is no need to indicate the last spin S_N since it is equal to the total spin S),

$$
{}^{\mathrm{K}}\Theta^{N}_{SM;k} = (S_1 S_2 \ldots S_{N-1}) \tag{19}
$$

The gradual formation of the Kotani spin functions and the values of f^N_S can be visualised by means of a Kotani branching diagram (Figure 2). Each circle in this diagram corresponds to an allowed value of the total spin S for a given number of electrons N. The spin function $(S_1 S_2 \ldots S_{N-1})$ is represented by the path which follows the arrows connecting the sequence of points $(1, S_1), (2, S_2), \ldots, (N, S)$. The number of all possible paths shown inside the circle at (N,S) is equal to f^N_S, and it is easy to establish that

$$
f^N_S = f^{N-1}_{S+1/2} + f^{N-1}_{S-1/2} \tag{20}
$$

The branching diagram allows the introduction of an alternative 'path' notation for the Kotani spin functions, given by the complete record of the directions of all upward and downward arrows (say, as a and b, respectively) connecting the origin $(0,0)$ and the final (N, S),

$$
{}^{\mathrm{K}}\Theta^{N}_{SM;k} = (c_{k_1} c_{k_2} \ldots c_{k_N}),\ c_{k_\mu} = \begin{cases} a & \text{if } S_{\mu-1} < S_\mu \\ b & \text{if } S_{\mu-1} > S_\mu \end{cases} \tag{21}
$$

This 'path' notation can be used in order to establish an ordering of the Kotani spin functions according to the so-called *last-letter* sequence [27]. If the first non-identical letters in the paths $(c_{k_1}c_{k_2}\ldots c_{k_N})$ and $(c_{l_1}c_{l_2}\ldots c_{l_N})$ are c_{k_μ} and c_{l_μ} (reading from right to left), then $(c_{k_1}c_{k_2}\ldots c_{k_N})$ is assumed to precede $(c_{l_1}c_{l_2}\ldots c_{l_N})$ if $c_{k_\mu} = b$. For example, the last-letter sequence ordering of the five Kotani spin functions for $N=5$ and $S=½$ is given by

$$\begin{aligned}
{}^{\mathrm{K}}\Theta^N_{SM;1} &= (aaabb)\\
{}^{\mathrm{K}}\Theta^N_{SM;2} &= (aabab)\\
{}^{\mathrm{K}}\Theta^N_{SM;3} &= (abaab)\\
{}^{\mathrm{K}}\Theta^N_{SM;4} &= (aabba)\\
{}^{\mathrm{K}}\Theta^N_{SM;5} &= (ababa)
\end{aligned} \tag{22}$$

The comparison between the Kotani spin functions in the last-letter ordering from Equation (22) to the leading terms which give rise to the Rumer spin functions from Equation (18) shows that the path notation for Kotani spin function k and that for the leading term $f^5_{1/2}+1-k$ are identical, except for the choice of letters. The same applies to any allowed combination of N and S values. Simonetta *et al.* [26] have established a simple relationship between the Rumer spin functions, constructed by means of the leading-term technique, and the Kotani spin functions, ordered in the last-letter sequence, according to which Schmidt orthogonalisation of ${}^{\mathrm{R}}\Theta^N_{SM;1}, {}^{\mathrm{R}}\Theta^N_{SM;2}, \ldots, {}^{\mathrm{R}}\Theta^N_{SM;f^S_N}$ produces ${}^{\mathrm{K}}\Theta^N_{SM;f^N_S}, {}^{\mathrm{K}}\Theta^N_{SM;f^N_S-1}, \ldots, {}^{\mathrm{K}}\Theta^N_{SM;1}$.

The Serber spin functions ${}^{\mathrm{S}}\Theta^N_{SM;k}$ are assembled consecutively from all four two-electron singlet and triplet spin functions

$$\begin{aligned}
&\Theta^2_{00} = 2^{-1/2}(\alpha\beta - \beta\alpha),\\
&\Theta^2_{1,-1} = \beta\beta, \quad \Theta^2_{10} = 2^{-1/2}(\alpha\beta + \beta\alpha), \quad \Theta^2_{1,-1} = \beta\beta
\end{aligned} \tag{23}$$

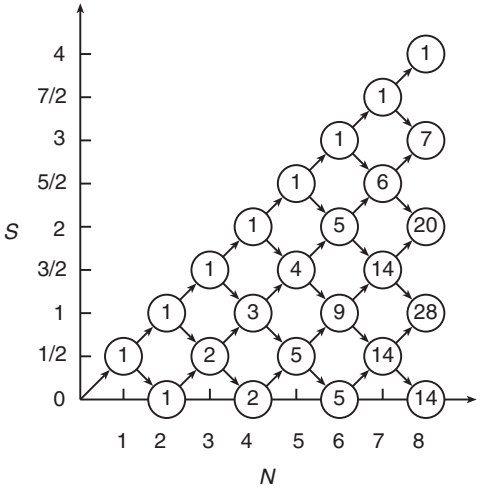

Figure 2. Kotani branching diagram.

When dealing with an odd number of electrons, it is also necessary to use the one-electron spin function for the last electron. Similarly to the case of the Kotani spin basis, the sequence of intermediate values of the total spin provides a compact notation for each Serber spin function

$$ {}^{S}\Theta^{N}_{SM;k} = \begin{cases} \underbrace{(\ldots((}_{N/2-1} s_{12}s_{34})S_4; s_{56})S_6; \ldots S_{N-2}; s_{N-1,N}) & \text{(for even } N\text{)} \\ \underbrace{((\ldots((}_{(N-1)/2} s_{12}s_{34})S_4; s_{56})S_6; \ldots S_{N-3}; s_{N-2,N-1})S_{N-1}) & \text{(for odd } N\text{)} \end{cases} \tag{24} $$

The pair spins $s_{\mu-1,\mu}$ take the values 0 or 1 depending on the singlet or triplet coupling of the spins of electrons μ and $\mu-1$. In the odd-electron case there is no need to record the spin of the last electron which has to be added to S_{N-1}, as it is always equal to ½.

The construction of the Serber spin functions can be visualised by means of a Serber branching diagram (Figure 3), which is similar in concept to a Kotani branching diagram (Figure 2). A two-electron triplet state can be added to a Serber spin function for $(N-2,S)$ in three different ways, illustrated by an upward arrow connecting $(N-2,S)$ to $(N,S+1)$, a downward arrow connecting $(N-2,S)$ to $(N,S-1)$ and a horizontal arrow connecting $(N-2,S)$ to (N,S), respectively (the last two arrows can be drawn only if $S>0$ at $N-2$). The addition of a two-electron singlet spin state to $(N-2,S)$ is denoted by a dashed horizontal arrow pointing from $(N-2,S)$ towards (N,S). The odd-electron spin states are connected to their even-electron precursors by upward and downward arrows, as in the case of the Kotani branching diagram. For even values of N, the relations involving successive values of f^N_S in the Serber spin basis take the form

$$ f^N_S = \begin{cases} f^{N-2}_{S+1} + f^{N-2}_{S-1} + 2f^{N-2}_S & \text{if } S>0 \\ f^{N-2}_{S+1} + f^{N-2}_S & \text{if } S=0 \end{cases} \tag{25} $$

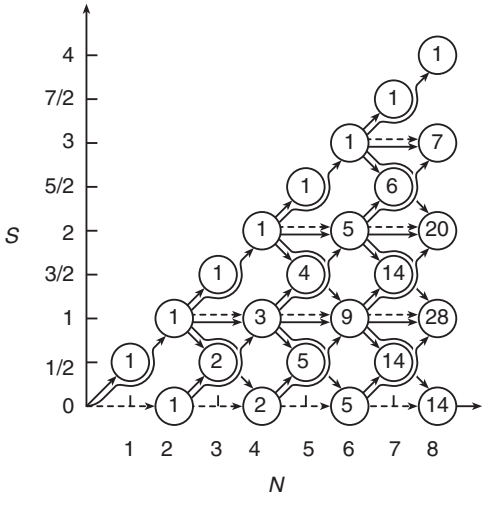

Figure 3. Serber branching diagram.

When N is odd, $f_S^N = f_{S+1/2}^{N-1} + f_{S-1/2}^{N-1}$, just as in the case of the Kotani spin basis [Equation (20)].

The Serber spin functions, similarly to the Kotani spin functions, are fully defined by the different paths on the Serber branching diagram. This allows the introduction of a corresponding 'path' notation

$$
\begin{aligned}
{}^{\mathrm{S}}\Theta_{SM;k}^{N} &= \begin{cases} (d_{k_1} d_{k_2} \ldots d_{k_{N/2}}) & \text{(for even } N\text{)} \\ (d_{k_1} d_{k_2} \ldots d_{k_{(N-1)/2}} c_{k_N}) & \text{(for odd } N\text{)} \end{cases} \\
d_{k_\mu} &= \begin{cases} A & \text{if } S_\mu = S_{\mu-2} \text{ and } s_{\mu-1,\mu} = 0 \\ B & \text{if } S_\mu = S_{\mu-2} + 1 \ (s_{\mu-1,\mu} = 1) \\ C & \text{if } S_\mu = S_{\mu-2} \text{ and } s_{\mu-1,\mu} = 1 \\ D & \text{if} S_\mu = S_{\mu-2} - 1 \ (s_{\mu-1,\mu} = 1) \end{cases}
\end{aligned}
\tag{26}
$$

(the symbol c_{k_N} has the same meaning as in the Kotani path notation [Equation (21)]).

The transformations between the representations of N-electron spin eigenfunction Θ_{SM}^N [Equation (2)] in the Kotani, Rumer and Serber spin bases

$$
\Theta_{SM}^N = \sum_{k=1}^{f_S^N} {}^{\mathrm{R}}C_{Sk}\,{}^{\mathrm{R}}\Theta_{SM;k}^N = \sum_{k=1}^{f_S^N} {}^{\mathrm{K}}C_{Sk}\,{}^{\mathrm{K}}\Theta_{SM;k}^N = \sum_{k=1}^{f_S^N} {}^{\mathrm{S}}C_{Sk}\,{}^{\mathrm{S}}\Theta_{SM;k}^N \tag{27}
$$

can be carried out in a straightforward manner with the use of a specialised code for symbolic generation and manipulation of spin eigenfunctions (SPINS, [28]). This code is also capable of calculating the changes in the spin-coupling coefficients induced by a reordering of the SC orbitals.

Probably the most convenient and widely accessible way of calculating fully-variational SC wave functions is based on the CASVB ideas for transforming CASSCF wave functions [15–19]. CASVB makes use of the fact that a CASSCF wave function, just like any full-CI construction, is invariant not only to a unitary but also to a general non-singular linear transformation of the active orbitals. This property can be exploited in order to transform this wave function to an alternative equivalent representation dominated by a small number of configurations. The transformation of the full-CI space induced by a non-unitary transformation of the orbital space can be carried out exactly by means of the efficient computational schemes developed in [16]. One straightforward application of the CASVB approach is associated with the generation of representations of a CASSCF wave function dominated by a single or multi configuration modern VB component. If we decompose a CASSCF wave function Ψ_{CAS} into a VB component Ψ_{VB} and its orthogonal complement within Ψ_{CAS}, $\Psi_{\mathrm{VB}}^{\perp}$, according to the equation

$$
\Psi_{\mathrm{CAS}} = S_{\mathrm{VB}}\Psi_{\mathrm{VB}} + (1 - S_{\mathrm{VB}}^2)^{1/2}\Psi_{\mathrm{VB}}^{\perp} \tag{28}
$$

the contribution of Ψ_{VB} to Ψ_{CAS} can be maximised by maximising the overlap-related quantity

$$
S_{\mathrm{VB}} = \frac{\langle \Psi_{\mathrm{CAS}} | \Psi_{\mathrm{VB}} \rangle}{\langle \Psi_{\mathrm{VB}} | \Psi_{\mathrm{VB}} \rangle^{1/2}} \tag{29}
$$

This procedure is relatively inexpensive computationally and, with reasonable choices for the form of Ψ_{VB}, it is fairly robust. An obvious alternative is to minimise the energy expectation value

$$E_{VB} = \frac{\langle \Psi_{VB}|\hat{H}|\Psi_{VB}\rangle}{\langle \Psi_{VB}|\Psi_{VB}\rangle} \tag{30}$$

The minimisation of E_{VB} is more expensive computationally than the maximisation of S_{VB}, because it requires evaluation of the Hamiltonian matrix element $\langle \Psi_{VB}|\hat{H}|\Psi_{VB}\rangle$ and its derivatives, but this may be achieved by adapting the efficient procedures already available in various CASSCF codes. It turns out, however, that if one employs the same VB *ansatz* within each of these two approaches, they tend to produce very similar Ψ_{VB} constructions which, in practice, makes the maximisation of S_{VB} the preferred procedure. Both optimisations utilise reliable Newton–Raphson-based techniques involving first and second derivatives.

The CASVB strategy for the fully-variational optimisation of modern VB wave functions relies on a linked two-step iterative strategy. Just as in CASSCF, this starts with choosing active and inactive spaces. An appropriate form for Ψ_{VB} must also be chosen. The first 'non-orthogonal' step involves the minimisation of E_{VB} using the CASVB algorithms, whereas the second 'orthogonal step' involves orbital optimisation using standard CASSCF procedures. When starting from a converged CASSCF wave function, convergence to a final VB wave function which has a high overlap with the CASSCF one (say, the SC wave function) can involve a very small number of iterations. This often makes the CASVB calculation of SC wave functions somewhat cheaper than the older traditional direct SC optimisation procedures [12,14]. The CASVB module is incorporated in MOLPRO [29] and in MOLCAS [30].

It is usual to benchmark the performance of a SC wave function with N active orbitals against an 'N in N' CASSCF construction. In the case of benzene, the amount of 'non-dynamic' '6 in 6' π space CASSCF correlation energy recovered by a SC wave function with six orbitals amounts to *ca.* 90% [31–33]. If SC theory is used to study the evolution of the electronic structure of a reacting system along a reaction path, the SC wave function accounts, as a rule, for more than 90% of the CASSCF correlation energy. In the case of the Diels–Alder reaction, the percentages are 92.9% at the transition state (TS), and 95.4% and 95.8% at the intrinsic reaction coordinate (IRC) geometries at $-0.6\,\text{amu}^{1/2}\text{bohr}$ and $0.6\,\text{amu}^{1/2}\text{bohr}$, respectively [34]. This shows that the single orbital product SC wave function can often provide a reasonably close approximation to its CASSCF counterpart, and it achieves that without the inclusion of ionic structures (i.e. those with one or more doubly occupied active orbitals), which feature so prominently in most applications of classical VB theory. The SC wave function may include smaller amounts of the CASSCF correlation energy for molecules in which the active orbitals are crammed together within a small volume of space. For example, for ethene ($H_2C{=}CH_2$) a SC wave function with four active orbitals engaged in two 'bent' bonds recovers 76.5% of the '4 in 4' CASSCF correlation energy, while for ethyne ($HC{\equiv}CH$) a SC wave function with six active orbitals engaged in three 'bent' bonds recovers 66.3% of the '6 in 6' CASSCF correlation energy [35].

A distinct advantage of the SC approach over other VB methods, especially those which retain more of the classical VB features, is that the SC wave function requires next

to no 'hand-tailoring'. In most cases, the input data for a SC calculation is similar to that for a CASSCF calculation and involves just choosing a suitable basis set, the numbers of core and active orbitals, and specifying initial guesses for these orbitals.

Similarly to MO-based approaches, such as Hartree–Fock and CASSCF, SC calculations can converge to wave functions corresponding to different local minima in terms of the variational parameters, some of which may not exhibit the full symmetry of the nuclear framework. Choosing appropriate initial guesses for the core and active orbitals is not always sufficient to ensure convergence to the lowest local minimum, or to a solution of the required symmetry. The SC codes described in [14] utilise a second-order constrained minimisation procedure which makes it straightforward to introduce simple orbital symmetry constraints such as

$$c_{p\mu} - \zeta_{p\mu qv}(R) c_{qv} = 0 \tag{31}$$

where $c_{p\mu}$ is the coefficient of basis function χ_p in orbital ψ_μ and $\zeta_{p\mu qv}(R)$ is a number associated with a symmetry operation R of the symmetry group of the molecule: it can take the values $0, \pm 1$. These simple symmetry constraints can help enforce σ–π separation in conjugated systems and achieve convergence to 'bent-bond' solutions in systems with multiple bonds [35]. Finding symmetry-adapted solutions for molecules that contain a symmetry axis of an odd order (say, C_3 or C_5) may require more general symmetry constraints of the form

$$c_{p\mu} - \sum_{q,v} \kappa_{p\mu qv}(R) c_{qv} = 0 \tag{32}$$

where the values of $\kappa_{p\mu qv}(R)$ are not restricted to $0, \pm 1$. Symmetry constraints of this type have been implemented in more recent versions of the SC codes described in [14]. Symmetry-constraint facilities are also available in CASVB [36].

While the use of symmetry constraints allows avoiding broken-symmetry solutions in the majority of cases, it is important to emphasise that, as discussed in detail in [37], VB wave functions that incorporate a single orbital product can be prevented from achieving the full symmetry of the problem by construction. In such situations, the only way to obtain a symmetry-adapted wave function is to use an appropriate symmetry projection operator which, when applied to a single orbital product VB wave function, produces a VB construction involving multiple orbital products.

One potential pitfall in SC calculations is associated with the fact that all SC orbitals ψ_μ in Equations (1) and (9) are non-orthogonal and there is no mechanism that would prevent three or more orbitals from trying to become the same during the variational optimisation of the wave function. This is in contrast to standard MO theory, where the orthogonality requirements allow no more than two spin-orbitals to be described by the same spatial component. When three or more SC orbitals become very similar, the antisymmetry requirement makes the norm of the SC wave function a very small number which can lead to a numerical instability in the optimisation procedure and a convergence failure. This situation, which can be aptly termed 'self-annihilation' of the SC wave function, is observed for some oxygen-containing systems, for example, formaldehyde ($H_2C{=}O$), in which an attempt to describe the carbon–oxygen double bond with a SC wave function with four active orbitals succeeds only if one imposes σ–π separation through appropriate orbital symmetry constraints. In an unconstrained calculation,

all four active orbitals 'collapse' onto the oxygen atom and the wave function optimisation fails to converge. In order to prevent the 'self-annihilation' of the SC wave function it would be necessary to find a way of ensuring that no more than two SC orbitals can become the same during the wave function optimisation procedure. A requirement of this type is far from straightforward to express analytically and to implement. Although the CASVB strategy appears to be more robust with respect to this SC wave function 'self-annihilation' than are direct codes [12,14], the problem is still not fully resolved. It is important to emphasise that there is nothing that prevents one or several pairs of SC orbitals from becoming the same. If two SC orbitals are identical, then all contributions to the N-electron spin eigenfunction Θ_{SM}^{N} [Equation (2)] from spin functions in which the spins of these two orbitals are triplet-coupled become equal to zero, and these two orbitals can be orthogonalised to all other SC orbitals (in other words, for all intents and purposes the two identical SC orbitals become core orbitals [Equation (9)].

The spin-coupled valence bond (SCVB) approach [38], which is a non-orthogonal CI expansion based on a SC reference, introduces a set of Fock-like one-electron operators, one for each occupied SC orbital. The eigenvalues of these Fock-like operators resemble orbital energies, and each occupied SC orbital usually represents the eigenfunction with the lowest eigenvalue of its Fock-like operator. The remaining eigenfunctions of each Fock-like operator form 'stacks' of virtual orbitals which can be used to construct additional configurations for the non-orthogonal CI expansion. It is usual to consider only 'vertical' excitations, in which an occupied SC orbital is replaced only by virtuals from its own 'stack'. As a rule, the orbitals from each 'stack' turn out to be localised within the same region of space which makes all excitations reasonably local. Perhaps the most successful application of this SCVB strategy to date is the extremely thorough study of all singlet and triplet valence excited states, as well as the $n = 3,4$ singlet and triplet Rydberg states of benzene below the first ionisation potential at 9.25 eV carried out in [39]. The use of the SCVB approach allowed the authors to classify the valence excited states as covalent or ionic in a straightforward manner, and it was shown that covalent states were well described using the usual assumption of σ–π separation. The errors in the computed transition energies to the ionic states were observed to be much larger, an indication that these states require additional σ–π correlation for their proper description. The use of a suitable σ core, derived from a calculation on the $C_6H_6^+$ cation, ensured very good descriptions of the Rydberg states. This work showed that compact and easy-to-interpret SCVB constructions are capable of describing excited states with numerical accuracy comparable to that of much larger Hartree–Fock- or CASSCF-based CI expansions.

3. Applications of SC theory to organic chemical reactions

3.1. *Background*

Early indications that SC theory could provide useful descriptions of organic reactivity were provided by studies of two reactions that involve singlet methylene (CH_2) [40,41]. To a first approximation, the SC description of singlet methylene resembles a standard VB description of CH_4, but with two of the hydrogen atoms missing. Such a description of the non-bonding electrons is entirely different from the description afforded by the simplest level of MO theory, in which these two electrons occupy a single orbital of a_1 (σ)

symmetry, but it is well known that reliable MO descriptions of this state require at least a two configuration description.

For the following reaction

$$H_2 + CH_2(^1A_1) \rightarrow CH_4$$

a SC study [41] of the simple symmetric approach of the two molecules, with the H_2 axis perpendicular to the C_2 axis of CH_2, suggests simultaneous breaking of the H–H bond and formation of the two new C–H bonds. Such a pathway does, however, appear to have a significant energy barrier. The form of the non-bonding orbitals for this state of CH_2 suggests that we could usefully consider an entirely different sort of path, in which both of the hydrogen atoms in H_2 initially move along the axis of one of the non-bonding orbitals. We found that as the distance from the carbon atom to the nearest incoming hydrogen atom decreases to *ca.* 3 bohr, the H–H bond begins to break and the first of the new C–H bonds begins to form. Simultaneously, the second hydrogen atom swings right around so as to interact with the other non-bonding orbital of CH_2, and it begins to form the second C–H bond. Although one of the C–H bonds starts to form before the other, this process is not completed before the second bond begins to form: overall, the process is synchronous. There appears to be no energy barrier along this path [41].

A preference for a non-symmetric path is also a hallmark of the SC description of the cycloaddition reaction of singlet methylene with ethene to form cyclopropane. For this system we considered the asymmetric approach with CH_2 impinging on one carbon atom of ethene, with the plane of the carbene twisted in order to maximise the overlap of one of its non-bonding orbitals with a p_π orbital of ethene [40]. In this way the initial attack of the soft electrophile (CH_2) is concentrated on a single position of the soft nucleophile (ethene). Ultimately, the new σ bonds which close the cyclopropane ring form in a single step according to the mechanism of a cheletropic reaction, and are consistent with the observation of a single stereoisomer in such reactions. Indeed, it is easy to detect the operation of a hook or claw in the evolution of the shapes of the SC orbitals [42].

Even when applied in an intentionally naïve fashion, SC theory can produce interesting insights into the way in which the reactants prefer to interact, as illustrated by the description of one of the simplest cycloaddition reactions, namely the orbital-symmetry-forbidden thermal dimerisation of two ethene molecules to cyclobutane [42]

$$2C_2H_4 \rightarrow C_4H_8$$

If we do not know anything about the mechanism of this reaction, one seemingly reasonable idea might be to bring the two ethene molecules together face to face, without even changing their geometries [Figure 4(a)].

The SC calculations for this mode of approach within the four-orbital active space sketched in Figure 4(a) produce a repulsive interaction curve. Even at separations close to typical single carbon–carbon bond lengths, the SC orbitals remain very similar to those in isolated ethene molecules, while the active space spin-coupling pattern is dominated by the reactant-like Rumer spin function (1–2,3–4). One obvious improvement is to allow the positions of the hydrogen atoms and the lengths of the carbon–carbon bonds within the two ethene moieties to relax with the decrease of the distance between the molecules. This leads to a SC potential curve that is lower in energy than that obtained with rigid geometries but, in agreement with the Woodward–Hoffmann rules, this new curve is

still repulsive. However, a closer look at the changes within the SC wave function as the ethene molecules approach one another reveals a clear hint about the nature of the actual path followed by this reaction. With the decrease of the distance between the reactants, the SC orbitals change in shape such that, instead of remaining engaged in a π bond within one of the two ethene moieties, each orbital starts to shift away from its π bond partner and towards the opposite orbital on the other reactant, as sketched in Figure 4(b). At the same time, the SC orbitals start to attain sp^3 character and to bend out of the rectangle formed by the carbon atoms. There is a parallel change in the active space spin-coupling pattern which gradually becomes dominated by the product-like Rumer spin function (1–3,2–4). All of this suggests the formation of a strained ring structure which is too high in energy to be able to influence the repulsive character of the potential curve. The ways in which the SC orbitals deform clearly indicate that the strain can be relieved by abandoning the concerted face to face approach and adopting a non-concerted reaction path leading to a *cis* or *trans* TS (Figure 4c and 4d).

In fact, as is shown in [42], a more consistent SC description of the cycloaddition of two ethene molecules requires use of eight SC orbitals. This arises because the reaction can be viewed as a rearrangement of four methylene radicals, each of which needs two active orbitals. An alternative justification is based on the utility of using a SC model of a single ethene molecule that includes four active orbitals engaged in two bent bonds [35]. In agreement with the MCSCF and MCSCF/MP2 results of Bernardi *et al*. [43], SC theory predicts that the *trans* pathway has a lower potential barrier and leads to a biradical intermediate of a lower energy. The minimum corresponding to the formation of a *cis* biradical intermediate is rather shallow. The SC interpretation for these reactions makes

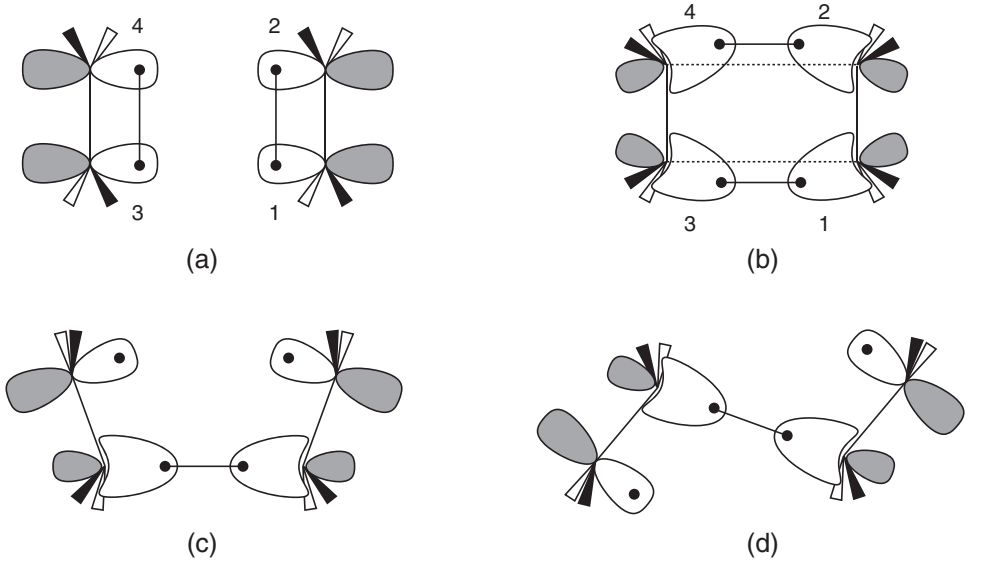

Figure 4. Naïve SC description of the orbital-symmetry-forbidden thermal cycloaddition of two ethene molecules: (a) face-to-face approach with fixed geometries, (b) face-to-face approach with optimised geometries, (c) end-to-end approach leading to a *cis* biradical, (d) end-to-end approach leading to a *trans* biradical.

use of the Serber spin basis and can be summarised as follows. The breaking of one of the two carbon–carbon bent bonds in each C_2H_4 and simultaneous re-engagement of two of the orbitals from the breaking bonds into a new carbon–carbon bond between the reactants leads to the formation of a *cis* or *trans* tetramethylene biradical. The remaining two electrons occupy distinctly non-bonding orbitals which resemble distorted carbon 2p AOs. In parallel, the coupling between the spins of the electrons occupying the orbitals involved in the breaking bonds changes from overwhelmingly singlet (within the separated ethene molecules) to predominantly triplet (within the tetramethylene biradicals). This picture, which closely resembles a dots and arrows scheme from a standard organic chemistry textbook, was another early indication of the potential of SC theory as a tool for interpreting the electronic mechanisms of chemical reactions.

The current procedure for constructing a SC model of the electronic mechanism of an organic chemical reaction involves two steps. Firstly, the TS and a sequence of geometries along the reaction path, also known as the IRC, in the directions of reactants and products, are calculated using an existing efficient implementation of an appropriate high-level MO theory or DFT approach. In principle, the transition structure can be optimised at the SC level of theory using the CASVB module in MOLPRO [29], but it is usually more convenient to use the efficient geometry optimisation and IRC algorithms implemented in GAUSSIAN [44], in conjunction with a more conventional approach such as CASSCF, MP2 or DFT. This first step is followed by a series of SC calculations at the geometries along the reaction path and a detailed analysis of the results of these calculations. Amongst other things, the analysis involves examining the variations in the shapes of the SC orbitals and the overlaps between, and the changes to the mode of spin coupling.

This methodology has provided new, interesting and often unexpected insights into the electronic mechanisms of a number of reactions, including the Diels–Alder reaction between butadiene and ethene [34], the hetero-Diels–Alder reaction of acrolein and ethene [45] and the retro Diels–Alder reaction of norbornene [46], the electrocyclicisation of cyclobutene to *cis*-butadiene [47], the disrotatory electrocyclic ring opening of cyclohexadiene to hexatriene [48], the 1,3-dipolar additions of fulminic acid to ethyne [49,50], of diazomethane to ethene [51] and of methyl azide to ethene [52], the electrophilic addition of hydrochloric acid to ethylene [53], S_N2 identity reactions [54], the addition reactions of singlet dihalocarbenes with ethene [55], the Claisen rearrangement of allyl vinyl ether [56], the $[1_s,5_s]$ hydrogen shift in (*Z*)-1,3-pentadiene [57] and the [1,3] sigmatropic rearrangement linking bicyclo[3.2.0]hept-2-ene and norbornene [58]. The SC models of these reactions have been shown to provide a theoretical vindication of the popular homolytic and heterolytic reaction schemes, drawn using half-arrows ('harpoons') and full-arrows, respectively, that can be found in many organic chemistry textbooks, in a context which is slightly different from the standard textbook interpretation, but makes very good sense from a quantum-chemical viewpoint. The half-arrows now indicate changes in the shapes of individual orbitals, accompanying the breaking of the bonds in which these orbitals participate in the reactants and their re-engagement in new bonds within the product, rather than movements of electrons; the full-arrows correspond to relocations of orbital, rather than electron pairs. An important feature of the SC models for the electronic mechanisms of pericyclic reactions is the possibility of identifying aromatic transition states, by looking for similarities with the well-known SC description of benzene [31,32,59].

3.2. *Diels–Alder reactions*

The SC description of the electronic mechanism of the Diels–Alder reaction between *cis*-butadiene and ethene [34] uses a wave function with six active orbitals in order to accommodate the four butadiene and two ethene π electrons involved in the bond-breaking and bond-formation processes.

The calculations show that throughout the reaction each orbital remains well-localised about one carbon atom. However, the sp^x character and the extent and direction of the deformation of each orbital towards other orbitals change considerably along the reaction path. Initially, the π bonds in butadiene are formed by the symmetry-related pairs of orbitals (ψ_1,ψ_2) and (ψ_3,ψ_4), while the pair (ψ_5,ψ_6) is responsible for the ethene π bond (see the right-hand column of orbitals in Figure 5 which shows the symmetry-unique SC orbitals ψ_1, ψ_2 and ψ_6 at a distance of 0.6 amu$^{1/2}$bohr along the reaction path from the TS towards the reactants). At the TS (see the middle column of orbitals in Figure 5), it is not difficult to notice that ψ_1 and ψ_6 are beginning to distort towards one another, while ψ_2 is beginning to distort towards its symmetry-related counterpart ψ_3. At the same time, there is an obvious decrease in the distortions (and overlap) linking ψ_1 and ψ_2. As shown in Figure 6(a), the overlaps between all SC orbitals participating in breaking and forming bonds become very much the same in the neighbourhood of the transition state. If we continue to follow the reaction path towards the product (see the left-hand column of orbitals in Figure 5), orbitals ψ_1 and ψ_6 become much more sp^3-like, and become engaged in one of the two new σ bonds formed during the reaction. Similarly, the pair of orbitals (ψ_2,ψ_3) becomes responsible for the newly-formed π bond.

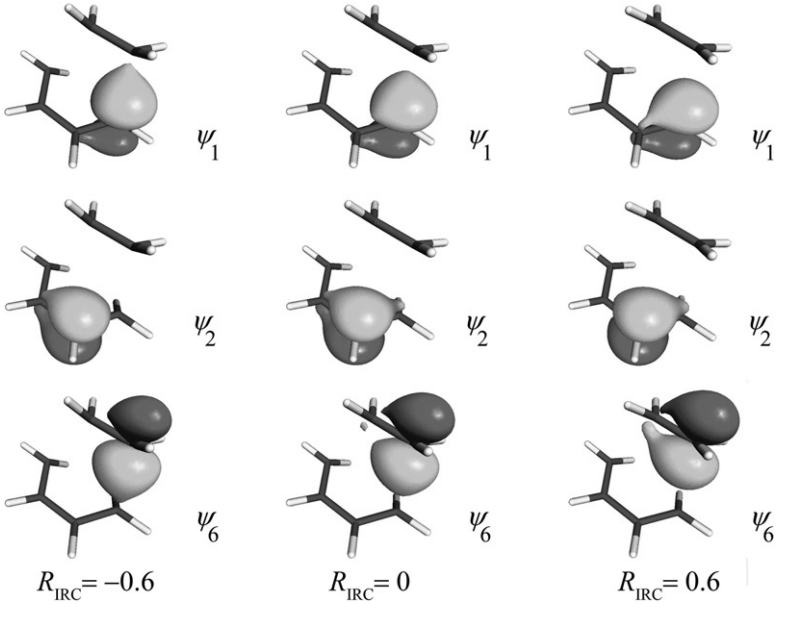

Figure 5. Symmetry-unique SC orbitals for the Diels–Alder reaction. Orbitals ψ_3, ψ_4 and ψ_5 can be obtained from ψ_2, ψ_1 and ψ_6 through reflections in the σ_h plane bisecting the ethene and central butadiene C–C bonds. Distances along the IRC are measured in amu$^{1/2}$bohr.

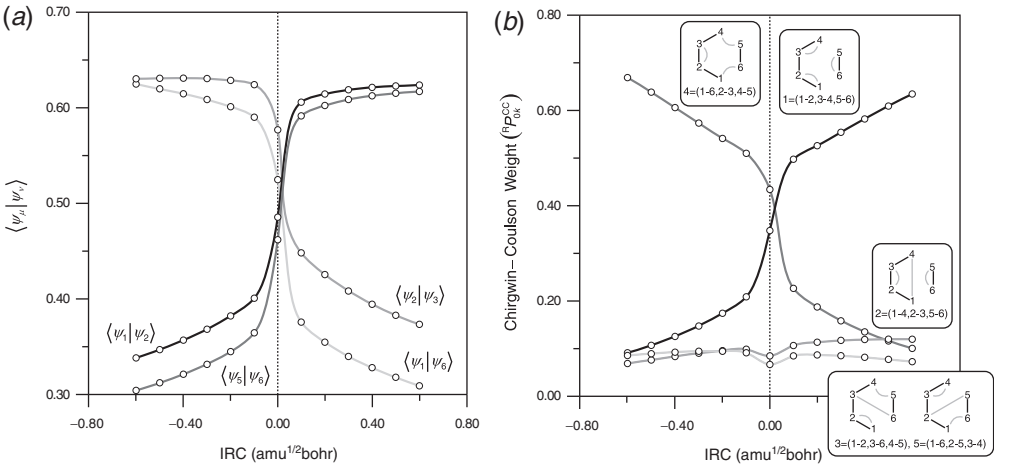

Figure 6. (a) Overlap integrals and (b) Spin-coupling weights for the Diels–Alder reaction.

The changes in the shapes of the SC orbitals are accompanied by a re-coupling of the electron spins. For this reaction, it proves most convenient to express the total active space spin function Θ_{00}^{6} in the Rumer basis. As can be seen in Figure 6(b), the two Kekulé-type spin eigenfunctions (1–2,3–4,5–6) and (1–6,2–3,4–5) dominate Θ_{00}^{6} throughout the reaction path. Function (1–2,3–4,5–6) reflects the spin-coupling pattern within the reactants, while (1–6,2–3,4–5) corresponds to the spin-coupling pattern within the product. The weights of these two Kekulé-like spin functions become equal in the vicinity of the transition state. At this stage the orbital overlaps, the mode of spin coupling and the estimated 'resonance energy' [34] indicate that the SC description of the reacting system is very similar to that of benzene [31,32,59], and so there are good reasons to regard the TS as aromatic. In this way, the SC study of the electronic mechanism of the Diels–Alder reaction [34] furnished the first evidence of an aromatic transition structure derived directly from the analysis of a post-Hartree–Fock wave function.

The changes in the SC orbitals and spin-coupling mode during the course of the reaction strongly suggest that the Diels–Alder reaction between *cis*-butadiene and ethene follows a homolytic mechanism that can be represented by Scheme A, in which six half-arrows indicate the simultaneous breaking of the three π bonds on the reactants and formation of the three new bonds, two σ and one π, in the product.

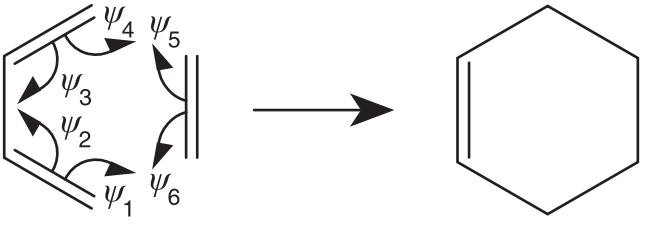

A

The SC description of the electronic mechanism of the hetero-Diels–Alder reaction of acrolein ($H_2C{=}CH{-}CH{=}O$) and ethene [45] was found to be very similar to that of the Diels–Alder reaction between *cis*-butadiene and ethene. Despite the fact that this concerted reaction is markedly asynchronous, with the breaking of the carbon–oxygen π bond, and the formation of the new carbon–oxygen σ bond, 'lagging behind' somewhat the other bond-making and bond-breaking processes, this reaction was found to proceed through a homolytic mechanism similar to that shown in Scheme A. Once again, it can be argued that soon after the transition state, following the reaction path in the direction of the product, the reacting system passes through a geometry at which it can be considered to be significantly aromatic.

More recently, a homolytic mechanism similar to that shown in Scheme A and involving a TS displaying aromatic features emerged from the SC description of yet another Diels–Alder reaction, namely the retro Diels–Alder reaction of norbornene leading to cyclopentadiene and ethene [46]. This is a strong indication that the homolytic mechanism in Scheme A and the aromatic TS represent general features of the SC model for the electronic mechanism of Diels–Alder reactions.

3.3. *Electrocyclic reactions*

The SC description of the conrotatory and disrotatory pathways in the electrocyclic isomerisation of cyclobutene to *cis*-butadiene [47] is one of the less successful applications of SC theory to chemical reactions. The main difference between the thermally-allowed conrotatory and thermally-forbidden disrotatory mechanisms was found to be, just as in the CASSCF case, the lower potential barrier for the conrotatory mechanism. Another difference is that, according to the SC model, at the conrotatory TS the reacting system exhibits considerable *cis*-butadiene character, which is an indication that the reaction is already well under way, while at the disrotatory TS the reacting system still remains predominantly reactant-like (i.e. similar to cyclobutene) which can be interpreted as a reluctance of the cycle to open in a disrotatory fashion. In both the conrotatory and disrotatory cases, the sharp changes in the weights of the two spin couplings, associated with the onset of bond breaking or bond formation, were observed to occur at IRC geometries well beyond the transition state. Although SC theory is capable of producing highly visual and easy-to-interpret descriptions of antiaromatic systems (see e.g. [60,61]), it was not possible to distinguish even traces of antiaromatic character in the SC wave functions for the conformations along the thermally-forbidden disrotatory pathway. This is not very surprising because antiaromaticity is a property which is much more elusive than aromaticity, especially if one is trying to find evidence for it in the results of *ab initio* calculations. However, in the absence of such evidence, SC theory fails to provide a simple qualitative explanation for the significant destabilisation of the disrotatory transition state.

Much more successful is the SC description of the disrotatory electrocyclic ring opening of cyclohexadiene to hexatriene [48]. Similarly to Diels–Alder reactions, a wave function with six SC orbitals is required. The changes in the symmetry-unique SC orbitals ψ_1, ψ_2 and ψ_3 along the reaction path are illustrated in Figure 7. Reflection of ψ_1, ψ_2 and ψ_3 in the symmetry plane retained throughout the reaction results in ψ_6, ψ_5 and ψ_4 respectively.

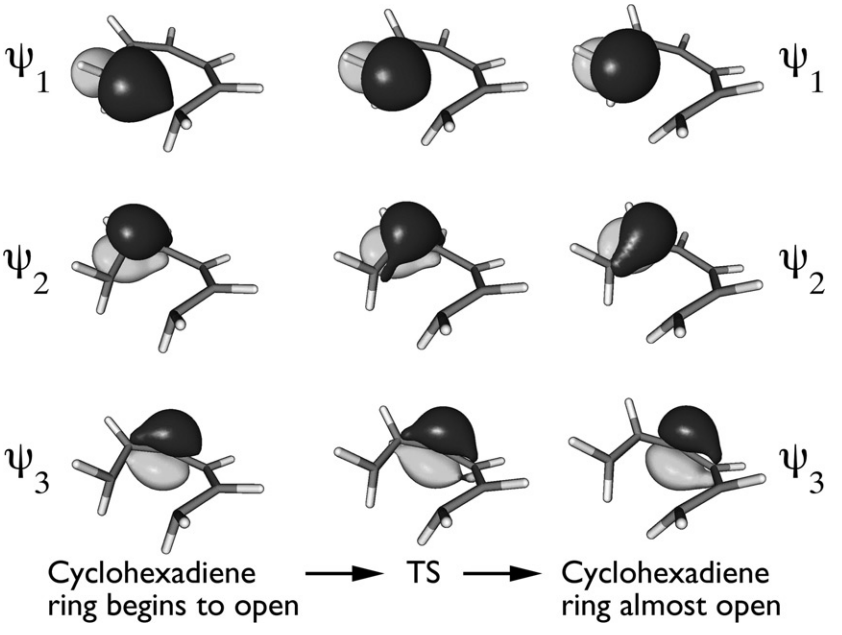

Figure 7. Symmetry-unique SC orbitals for the disrotatory electrocyclic ring-opening of cyclohexadiene.

When the cyclohexadiene ring begins to open (see the leftmost column of orbitals in Figure 7), ψ_1 and ψ_6 still take the form of sp^x-like hybrids with significant s character. The pairs (ψ_2,ψ_3) and (ψ_4,ψ_5) account for the π bonds in the cyclohexadiene ring. At the TS (middle column in Figure 7) orbitals ψ_2–ψ_5 are starting to attain much the same 'symmetrically-distorted' shape as orbital ψ_2 at the Diels-Alder TS (Figure 5). The increased distance between the two terminal atoms is reflected in less distortion of ψ_1 and ψ_6 towards one another, and a reduced overlap. However, for this system, the most dramatic changes in the orbital overlaps and in the mode of spin coupling occur a little after the TS (Figure 8), when the carbon–carbon bond lengths in the chain become almost equal. The near-perfect 'resonance' of two Kekulé-type modes of spin coupling, namely the reactant-like (1–6,2–3,4–5) and product-like (1–2,3–4,5–6), as well as the near equalisation of bond lengths and of orbital overlaps, suggests that this is another reaction that passes through an 'aromatic' structure.

When the ring opening is approaching completion, the distance between the terminal carbon atoms is significantly larger and orbitals ψ_1 and ψ_6 are now essentially π orbitals. The three π bonds are accounted for by the pairs (ψ_1,ψ_2), (ψ_3,ψ_4) and (ψ_5,ψ_6), and the related Kekulé-type mode of spin coupling (1–2,3–4,5–6) becomes the most important, as shown in Figure 8(b).

The orbitals remain associated with the same carbon atom throughout the reaction, but there is a recoupling of the corresponding electron spins. As in the case of the Diels–Alder reaction, it seems appropriate to label the changes as 'homolytic', as might be represented by the simplistic representation in Scheme B. One difference from the Diels–Alder reaction, however, is that for this reaction the aromatic structure occurs a little after the TS [48].

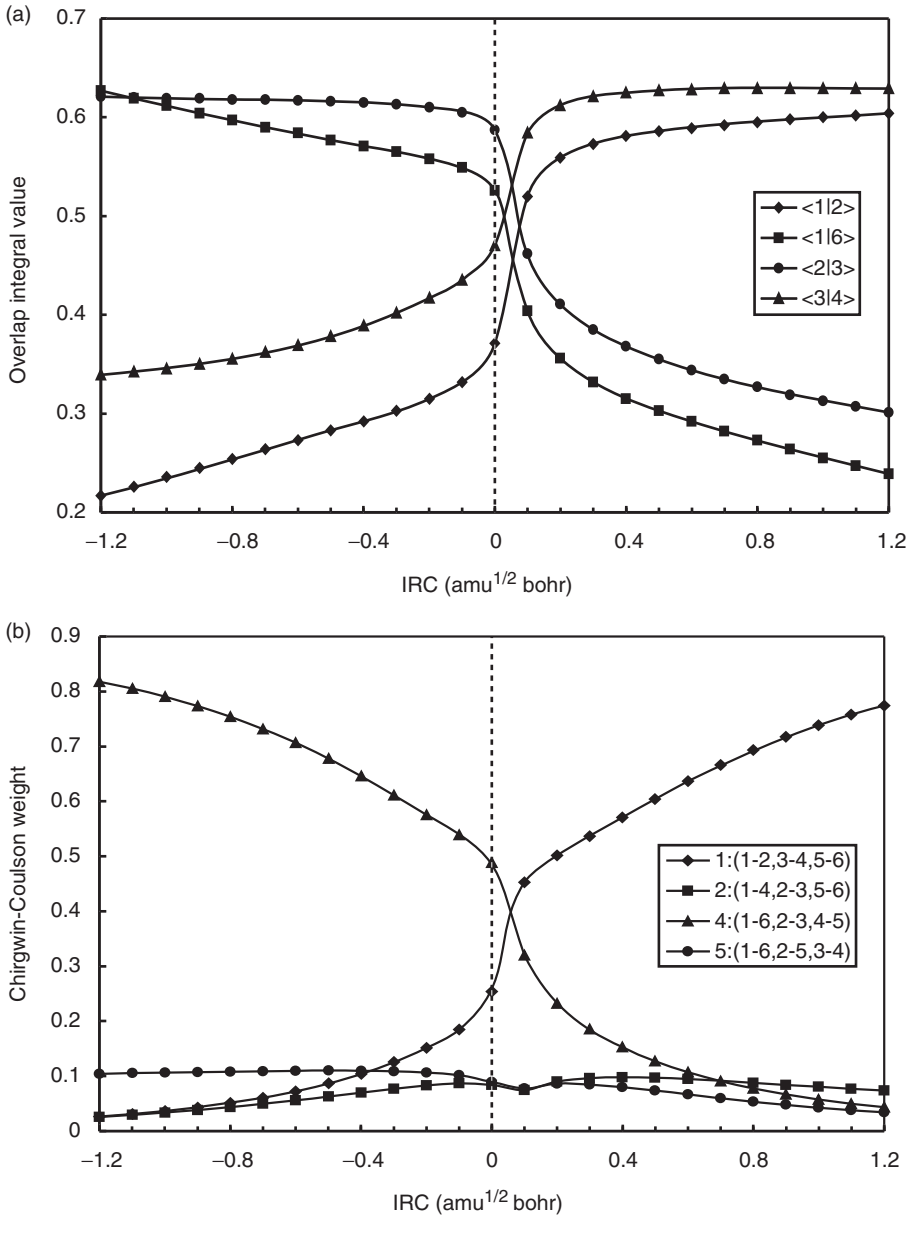

Figure 8. (a) Overlap integrals and (b) spin-coupling weights for the disrotatory electrocyclic ring-opening of cyclohexadiene.

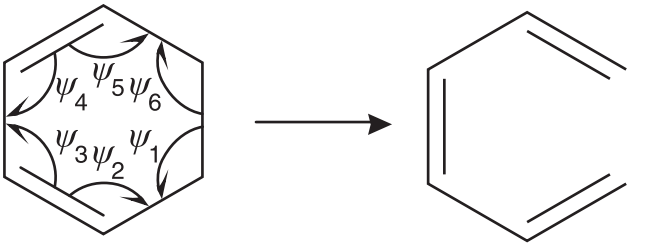

B

3.4. *1,3-Dipolar cycloaddition reactions*

The nature of the electronic rearrangements that take place during 1,3-dipolar cycloaddition reactions has been a long-standing debating point amongst theoretical chemists. In the case of the 1,3-dipolar cycloaddition reaction between fulminic acid and ethyne, both SC [49] and restricted Hartree–Fock (RHF) [62,63] treatments suggest a heterolytic mechanism illustrated by Scheme C1 which involves the movement of electron pairs that are retained throughout the course of the reaction (the N to O arrow indicates that the corresponding N–O π bond is strongly polarised towards the oxygen atom). However, in the case of the 1,3-dipolar cycloaddition reaction involving diazomethane and ethene, the SC analysis [51] produces Scheme D, whereas RHF theory [62,64,65] suggests an electron flow in the opposite direction, of the type illustrated by Scheme C2.

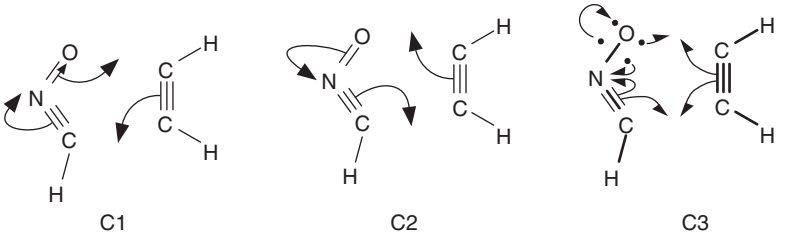

C1 C2 C3

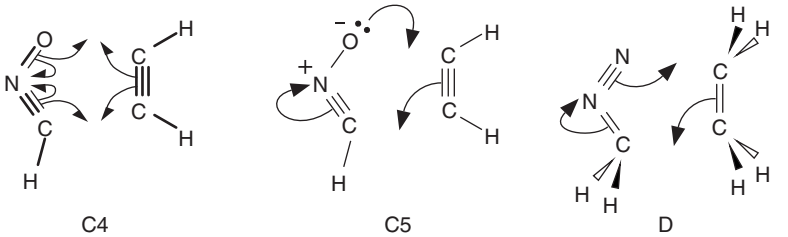

C4 C5 D

Nguyen *et al*. [66] argued that the 1,3-dipolar cycloaddition reaction between fulminic acid and ethyne should be described by Scheme C2. Two approaches were used, the first of which, CI-LMO-CAS, involves localisation of the '6 in 5' CASSCF active space orbitals and analysis of the weights of the configurations when expressed in terms of these localised orbitals. However, the two configurations, which were thought to be

responsible for the reaction mechanism, do not dominate the CASSCF wave function: they have a combined weight that never exceeds *ca.* 44%. The '6 in 5' active space requires one of the active orbitals to be doubly-occupied and this orbital localises around the more electronegative atoms, O and N, which explains the direction of the leftmost arrow in Scheme C2. It is also possible to voice concerns about the predictive power of the second approach, which was based on the application of DFT-based reactivity descriptors to fulminic acid, not least because it examined an isolated molecule which was 'unaware' of the presence of the other reactant and had a linear equilibrium geometry, very different from its conformation near the transition state.

Harcourt's qualitative classical VB analysis [67] led to the formulation of a 'concerted biradical' mechanism for 1,3-dipolar cycloaddition reactions (see also [68] and references therein). This combination of terms may sound unusual to those dealing with pericyclic reactions (as a rule, within the accepted terminology, 'biradical mechanism' is synonymous with a non-concerted, stepwise mechanism involving a biradical intermediate), but in this instance 'biradical' was used to denote a homolytic electronic rearrangement. Harcourt and Schulz [69] also discussed possible homolytic mechanisms for the 1,3-dipolar cycloaddition reaction between fulminic acid and ethyne. These mechanisms are illustrated by Schemes C3 and C4. The dots on the two sides of the O–N bond in C3 correspond to singly-occupied π_x(ON) and π_y(ON) localised MOs, while the thick and thin lines in C3 and C4 represent 'normal' and 'fractional' 'electron-pair bonds' in Harcourt's notation. According to Harcourt and Schulz, the preferred scheme should be Scheme C3. The presence of mutually perpendicular π localised MOs in this scheme follows from the fact that the analyses of the reaction mechanisms corresponding to C3 and C4 in [69] were based on the electronic structure of HCNO at its linear gas phase equilibrium geometry and did not take into account the presence of the second reactant and the changes in the geometry of the reacting system along the reaction path. As a rule, the wave functions used by Harcourt and co-workers are molecule-specific, carefully hand-crafted VB constructions which are defined within a fairly minimal set of basis functions. Wave functions of this type cannot ordinarily be expected to provide a consistent picture of electronic structure changes along a general reaction path, because the hand-tuning required at different points along this path might well produce different wave function constructions. Harcourt and Schulz criticised Scheme C1 (and, effectively, Scheme C2) stating that this scheme should involve charge transfer between the species. This is not correct. The 1,3-dipolar cycloaddition reaction between fulminic acid and ethyne is a concerted, almost synchronous process and so all electron rearrangements depicted by Schemes C1 and C2 take place simultaneously, without any noticeable charge transfer between the reactants. Although the terms 'heterolytic' and 'homolytic' can be used to distinguish between mechanisms C1 and A, these do not imply the existence of any biradical or zwitterionic intermediates [34].

Sakata [70] carried out a Hartree–Fock-level population analysis along the reaction path of the 1,3-dipolar cycloaddition reaction between fulminic acid and ethyne. His results suggest a mechanism described by Scheme C5, which is very similar to C1 and in line with previous Hartree–Fock-level results.

In a discussion about the existing models for the electronic mechanism of the $HCNO + C_2H_2$ 1,3-dipolar cycloaddition reaction that was initiated by Nguyen *et al.* [71] (see also the replies [50,68]), those authors claimed that the contrast between the

predictions coming from two very different VB treatments (compare Scheme C1 [49] to C3 and C4 [69]) was an indication that VB theory was unable to provide credible coherent results about the electronic structure rearrangements that take place during 1,3-dipolar cycloaddition reactions. In fact, although the results of the existing SC calculations had suggested the heterolytic mechanisms C1 and D for the 1,3-dipolar cycloaddition reactions between fulminic acid and ethyne, and diazomethane and ethene, respectively, there are no restrictions within the wave function *ansatz* which would prevent SC theory from predicting homolytic mechanisms for other 1,3-dipolar cycloaddition reactions. This was confirmed by the SC analysis of the electronic mechanism of the 1,3-dipolar cycloaddition reaction between methyl azide (CH_3N_3) and ethene [52] which showed that this reaction should follow a homolytic mechanism.

It is informative to examine and to compare the most important features of the heterolytic and homolytic mechanisms proposed by SC theory for the 1,3-dipolar cycloaddition reactions between fulminic acid and ethyne [49], and between methyl azide and ethene [52]. The changes in the shapes of the six SC orbitals during the 1,3-dipolar cycloaddition of fulminic acid to ethyne are illustrated in Figure 9. When the reacting molecules are far apart (see the rightmost column of orbitals in Figure 9), the orbitals on HCNO (ψ_1, ψ_3, ψ_5 and ψ_6) reproduce the well-known SC model for the electronic structure of 1,3-dipoles, in which the central heavy atom can be considered 'hypervalent' (see e.g. [72,73]). The nitrogen atom in HCNO appears to take part in more than four covalent bonds: an almost triple bond between C and N (ψ_3 and ψ_6 account for one of the components of this bond, which is of σ symmetry in linear HCNO), a π bond between N and O and a highly polar bond between N and O (of σ symmetry in linear HCNO, described here by orbitals ψ_1 and ψ_5). The remaining two orbitals, ψ_2 and ψ_4, form the ethyne bond (of π symmetry in linear C_2H_2) that breaks during the reaction.

A clear representation of the spin-coupling pattern at this stage of the cycloaddition process can be achieved by reordering the SC orbitals so as to put in pairs the orbitals involved in the three bonds: ψ_2 and ψ_4, ψ_6 and ψ_3, and ψ_5 and ψ_1. The spin-coupling pattern for the reordered orbital set is largely dominated by its 'perfect-pairing' component (in the Kotani spin basis ${}^{K}\Theta^{6}_{00;5} = (\frac{1}{2}0\frac{1}{2}0\frac{1}{2})$), in which the orbital pairs (ψ_2,ψ_4), (ψ_6,ψ_3) and (ψ_5,ψ_1) are singlet-coupled. The composition of the spin-coupling pattern changes very little throughout the cycloaddition process; this indicates that these orbital pairs are preserved all the way from reactants to product. One of the orbitals within each of the orbital pairs (ψ_2,ψ_4) and (ψ_5,ψ_1) undergoes profound changes along the reaction path. Orbital ψ_2, which starts as one of two orbitals involved in the in-plane ethyne 'π' bond, becomes at the TS a linear combination of two sp^x hybrids, one at its 'original' ethyne carbon atom, and another one at the HCNO carbon atom. After the transition state, this orbital moves away from the ethyne carbon atom and it localises onto the HCNO carbon atom. The other orbital within this pair, ψ_4, experiences extensive 're-hybridisation'. As a result, after the TS (see the leftmost column in Figure 9), orbitals ψ_2 and ψ_4 become responsible for one of the two bonds closing the isoxazole ring. Orbital ψ_5 starts as one of the orbitals from the in-plane polar 'π' N–O bond in HCNO, but at the TS it becomes, similarly to orbital ψ_2, a mixture of two sp^x hybrids, one of which is at its original location (the oxygen atom) and the other one is at the approaching ethyne carbon atom. After the transition state, this orbital shifts to a large extent to the ethyne carbon atom. The second orbital in this pair, orbital

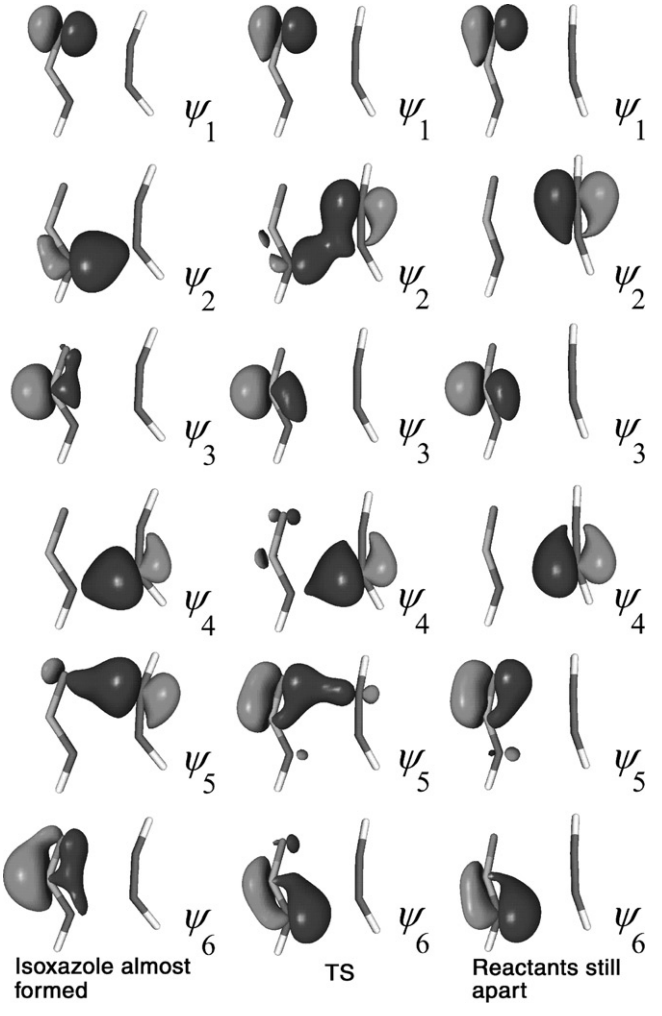

Figure 9. Shapes of the six SC orbitals at different stages of the 1,3-dipolar cycloaddition of fulminic acid to ethyne.

ψ_1, changes very little throughout the reaction. After the transition state, orbitals ψ_5 and ψ_1 form the second bond closing the isoxazole ring. The orbitals from the pair (ψ_6,ψ_3) are initially engaged in the in-plane C–N 'π' bond in HCNO. Both orbitals remain largely static, moving just enough so as to form, by the end of the reaction, a non-bonding pair on the isoxazole nitrogen atom, partially polarised towards the oxygen atom.

The fact that, throughout the part of the reaction path studied at the SC level of theory, the active space spin-coupling pattern remains dominated by a single component, indicates that there is no significant resonance that could be associated with aromatic properties. Thus, it is safe to assume that the reacting system remains non-aromatic throughout the course of the reaction.

The orbital pair shifts responsible for the bonding rearrangements associated with the 1,3-dipolar cycloaddition of fulminic acid to ethyne can be summarised through the homolytic Scheme C1 in which the leftmost, middle and rightmost arrows depict the shifts of (ψ_6,ψ_3), (ψ_5,ψ_1) and (ψ_2,ψ_4), respectively. Apart from some relatively minor differences in the 'timelines' of changes in the shapes of some of the orbitals along the reaction path, the essential features of this mechanism are repeated in the SC analysis of the 1,3-dipolar cycloaddition reaction between diazomethane and ethene (Scheme D) [51].

The SC descriptions of the electronic mechanisms of the 1,3-dipolar cycloaddition reaction between fulminic acid and ethyne, and between diazomethane and ethene involve bond rearrangements, achieved through the movement of singlet orbital pairs through space, during which at least one of the orbitals within a pair becomes completely detached from the atomic centre with which it was associated initially and ends up localised around another centre. The ability of the SC wave function to produce a description of this type follows from the fact that the SC orbitals are singly-occupied non-orthogonal functions. A classical-style VB approach, which makes use of orbitals strictly associated with atomic centres, would need a number of additional and, in this case, rather unphysical, ionic structures in order to compensate for the insufficient flexibility of these orbitals along the reaction path.

The SC wave function used to describe the electronic mechanism of the 1,3-dipolar cycloaddition reaction between methyl azide and ethene involves eight active orbitals [52]. The changes in the shapes of the SC orbitals during this reaction are illustrated in Figure 10. At the 'before transition state' geometry (see the top group of orbitals in Figure 10), the pair (ψ_4,ψ_5) corresponds to the ethene π bond, while the remaining six orbitals are all on the methyl azide. The pair (ψ_1,ψ_6) is responsible for the nearly π bond between the central nitrogen atom and the N atom connected to the methyl group, while the two nearly π bonds between the central and terminal nitrogen atoms are described by the orbital pairs (ψ_2,ψ_3) and (ψ_7,ψ_8). The 'before transition state' active space spin-coupling pattern is strongly dominated by reactant-like Rumer spin functions, which couple to singlets the spins of orbitals residing on the same reactant only. Of these, the most important one is (1–6, 2–3, 4–5, 7–8), which is in line with the assignments of orbital pairs to bonds.

The shapes of the orbitals at the TS (see the middle group of orbitals in Figure 10) are more product-like. Two new pairs, (ψ_3,ψ_4) and (ψ_5,ψ_6), reflect the formation of the two new bonds closing the ring, whereas ψ_1 and ψ_2 are about to become responsible for the lone pair on the central nitrogen in the product, while ψ_7 and ψ_8 now clearly form the almost π component of the N=N bond. The main contribution to the active space spin-coupling pattern now comes from the Rumer spin eigenfunction (1–2, 3–4, 5–6, 7–8) in which the spins of all pairs of active orbitals which are becoming involved in bonds or in the central nitrogen lone pair in the product are coupled to singlets. Second in importance is the Rumer spin eigenfunction (1–2, 3–6, 4–5, 7–8) which, in contrast to the function (1–2, 3–4, 5–6, 7–8), is reactant based. It couples to singlets the spins of the active orbitals that are becoming engaged in the central nitrogen lone pair (ψ_1,ψ_2), the orbitals that were initially involved in the ethene π bond (ψ_4 and ψ_5), the orbitals that initially described one of the components of the N≡N bond in methyl azide and, later, the almost π component of the N=N bond in the product (ψ_7 and ψ_8), and of the two orbitals which reside on different ends of the 1,3-dipole (ψ_3 and ψ_6).

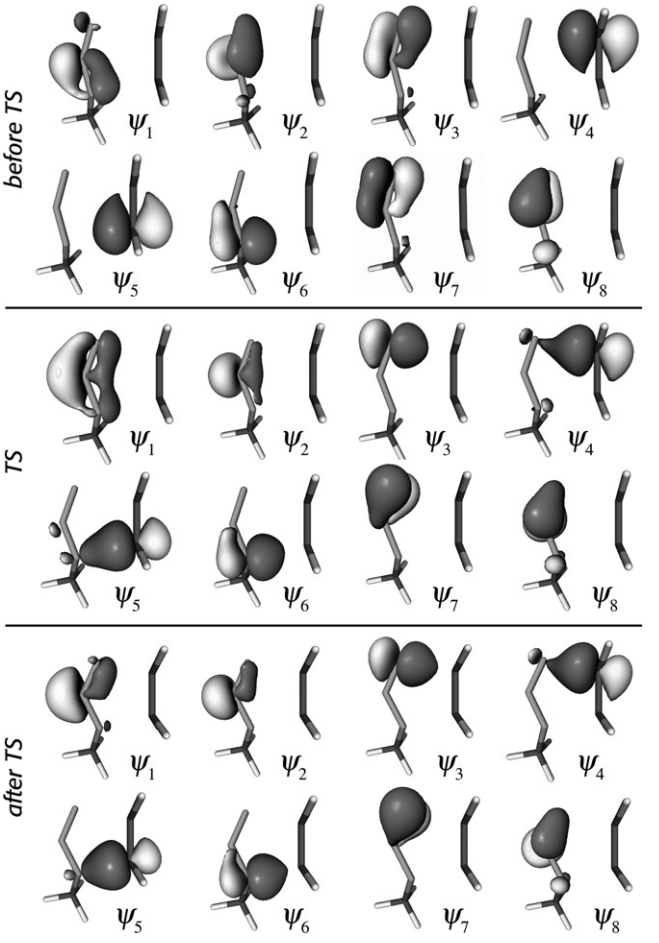

Figure 10. SC orbitals at various stages of the 1,3-dipolar cycloaddition of methyl azide to ethene.

As the reactants approach one another, the weight of Rumer spin function (1–2, 3–6, 4–5, 7–8) starts to increase, in parallel with the decrease of the weight of spin function (1–6, 2–3, 4–5, 7–8), and it peaks near the transition state. This finding, in combination with the observed changes in the shapes of the valence orbitals and their overlaps indicates that, on approaching the transition state, the bonds realised by the orbital pairs (ψ_1,ψ_6) and (ψ_2,ψ_3) gradually weaken; this is accompanied by the formation of a lone pair on the central nitrogen, represented by the singlet-coupled orbitals ψ_1 and ψ_2. As the new bonds involving ψ_3 and ψ_6 are not yet fully developed, the active space spin function in the vicinity of the TS displays competition (or 'resonance') between two spin-coupling patterns: the product-like (1–2, 3–4, 5–6, 7–8) and the reactant-based (1–2, 3–6, 4–5, 7–8). These patterns differ only in the mode of coupling of the spins of the four orbitals responsible for the two new bonds closing the ring: ψ_3, ψ_4, ψ_5 and ψ_6. The large spatial separation and the low overlap between orbitals ψ_3 and ψ_6 suggests that the

presence of the less important pattern (1–2,3–6,4–5,7–8) is an indication that the reacting system attains, near the transition state, some singlet biradical character. However, there is no hint of the benzene-like 'resonance' that is observed near the transition states of the Diels–Alder reaction between butadiene and ethene [34] and for the electrocyclisation of hexatriene [48].

The 'after transition state' SC picture (see the bottom group of orbitals in Figure 10) shows a further development of the product-like features observed at the transition state. The only particularly noticeable changes in the forms of the SC orbitals are some 'compacting' of the lone pair orbitals ψ_1 and ψ_2. The active space spin-coupling pattern is largely dominated by the product-like function (1–2,3–4,5–6,7–8), while the weight of the reactant-based singlet biradical pattern (1–2,3–6,4–5,7–8) becomes so low that it is safe to ignore its contribution.

Throughout the 1,3-dipolar cycloaddition reaction of methyl azide with ethene, each SC orbital remains distinctly associated with a single atom while its form, overlap with other SC orbitals and participation in the active space spin-coupling pattern adjust to accommodate the differences in the nature of the bonding in the reactants and product. The bond-breaking and bond-formation processes realised in this way can be illustrated through a homolytic scheme (Scheme E) which is similar to Scheme C4.

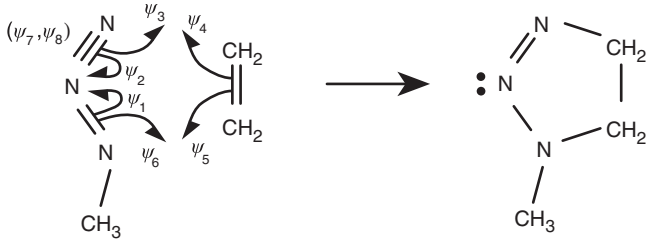

E

3.5. *Sigmatropic rearrangements*

Various geometric, energetic and magnetic criteria strongly suggest that the transition structure of the [1,5]-H shift in *Z*-1,3-pentadiene is aromatic [74,75]. As a consequence, it would have been reasonable to expect that the SC description of this reacting system near the TS would show benzene-like features and that it would very much repeat the picture observed for the prototypical Diels–Alder reaction [34]. In fact, the SC description of the TS of the [1,5]-H shift in *Z*-1,3-pentadiene [57] turns out to be markedly different. The active space is found to involve two strongly interacting three-orbital moieties, one of which (centred on the carbon atom opposite the shifting hydrogen atom) is almost identical to the three-orbital 'antipair' SC picture of the π active space in the allyl radical [76], while the second one (centred on the shifting hydrogen) is very similar in nature, but involves more σ-like orbitals. However, in previous SC work 'antipairs' had often been associated with antiaromaticity and radical or diradical character (see e.g. the SC description of square cyclobutadiene [60]). The detailed analysis carried out in [57] showed that, on their own, 'antipairs' should not in fact be considered as a sign of antiaromaticity or diradical character, as these can be observed even within an alternative π space SC wave function for benzene. Indeed, 'antipairs' can be expected to appear within the SC descriptions of reactions which follow heterolytic mechanisms (involving movements of

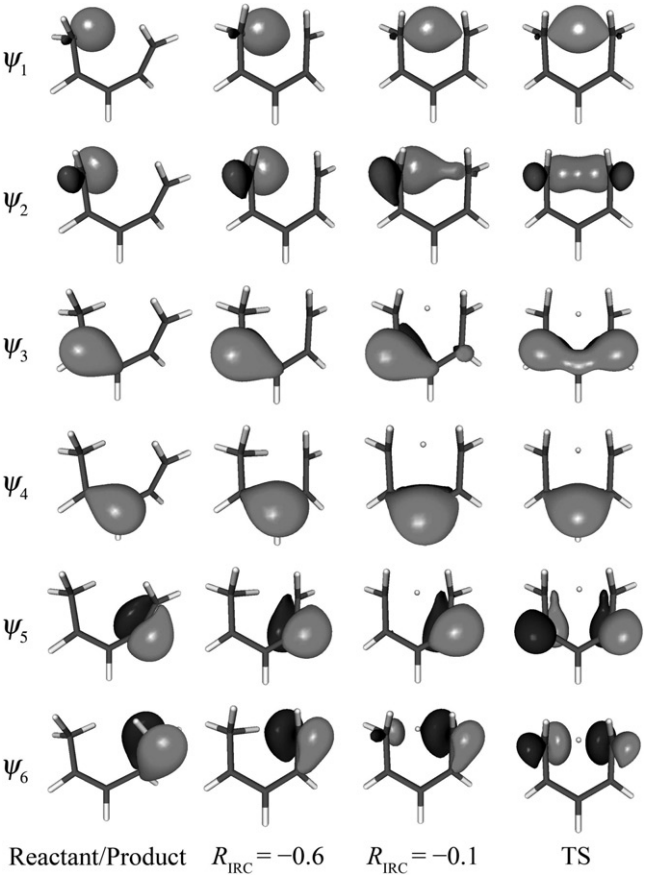

Figure 11. SC orbitals at various stages of the [1,5]-H shift in *Z*-1,3-pentadiene. Distances along the IRC in amu$^{1/2}$bohr.

orbital pairs) and pass through aromatic transition states; this was observed for the first time in the SC study of the [1,5]-H shift in *Z*-1,3-pentadiene.

The [1,5]-H shift in *Z*-1,3-pentadiene is a degenerate pericyclic process for which the IRC is symmetric with respect to the transition state. As a result, it is sufficient to examine the changes in the SC wave function along just one of the two possible directions starting at the transition state. The shapes of the six SC orbitals at the reactant geometry (which coincides with that of the product), at two intermediate IRC geometries, and at the TS are shown in Figure 11.

At the reactant/product geometry (see the leftmost column in Figure 11), the six SC orbitals are engaged in three well-defined bonds. The pair (ψ_1,ψ_2) is responsible for the σ bond attaching the hydrogen atom that migrates during the course of the reaction from the leftmost carbon atom (C_1) to the rightmost carbon atom (C_5), while the remaining two pairs, (ψ_3,ψ_4) and (ψ_5,ψ_6), describe the diene π bonds.

During the course of the reaction both orbitals from the pair (ψ_1,ψ_2) develop distortions towards C_5. Orbital ψ_1 remains associated with the migrating H atom while,

by the end of the reaction, its partner ψ_2 shifts from C_1 onto C_5. At the transition state, ψ_2 looks very much like the in-phase superposition of two sp^3-like hybrids, based on C_1 and C_5. The changes within orbital pair (ψ_3,ψ_4) closely parallel those within (ψ_1,ψ_2): ψ_4 remains attached to C_3, while ψ_3 relocates from C_2 onto C_4. At the transition state, ψ_1, ψ_2, ψ_3 and ψ_4 are symmetric with respect to the σ_h plane passing through C_3 and the migrating H atom. Away from the transition structure the pair (ψ_5,ψ_6) is responsible for a π bond (C_4–C_5 in the reactant, and C_1–C_2 in the product). At the transition state, ψ_5 and ψ_6 are semilocalised over two atomic centres and both orbitals are antisymmetric with respect to the σ_h plane. The composition of the spin-coupling pattern and the orbital overlaps clearly indicate that the orbital pairs (ψ_1,ψ_2), (ψ_3,ψ_4) and (ψ_5,ψ_6) are preserved throughout the reaction path. The movements of these three orbital pairs during the [1,5]-H shift in (*Z*)-1,3-pentadiene can be described using Scheme F,

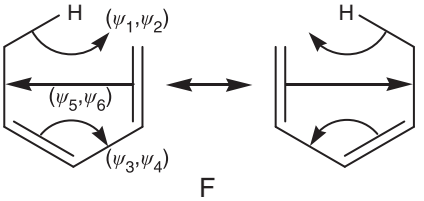

F

which suggests that the reaction proceeds through a heterolytic mechanism that is markedly different from that depicted in the textbook-style Scheme G.

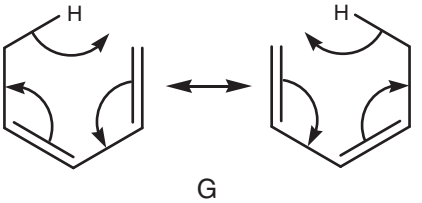

G

Scheme F involves an unusually long-range relocation of orbital pair (ψ_5,ψ_6) which, at first glance, is difficult to accept. However, a closer examination of Scheme G shows that the required movements of the orbital pairs responsible for the diene π bonds cannot be described by a SC wave function which reproduces the C_s symmetry of the transition structure. The shifts of orbital pairs (ψ_1,ψ_2) and (ψ_3,ψ_4) shown in Scheme F are consistent with the C_s symmetry of the transition structure, but then the only option left to (ψ_5,ψ_6) is to relocate across the ring.

Further insights into the electronic structure of the TS for the [1,5]-H shift in (*Z*)-1,3-pentadiene, can be gained by reordering the orbitals in the SC wave function as

$$\Psi_{00}^{6} = \hat{A}[(core)\psi_1\psi_2\psi_3\psi_4\psi_5\psi_6\Theta_{00}^{6}] = \hat{A}[(core)\psi_2\psi_6\psi_1\psi_4\psi_3\psi_5\Theta_{00}^{6\,\prime}] \tag{33}$$

where

$$\Theta_{00}^{6\,\prime} = \sum_{k=1}^{5} {}^{S}C_{0k}{}' \, {}^{S}\Theta_{00;k}^{6} \tag{34}$$

stands for the spin-coupling pattern corresponding to the new ordering of the SC orbitals, expressed in the Serber spin basis. This new ordering of the SC orbitals allows the identification of two 'antipairs', involving orbitals ψ_3 and ψ_5, and ψ_2 and ψ_6, respectively. The spins of the orbitals from an 'antipair' are almost entirely triplet-coupled, which is not easy to notice within a spin basis other than the Serber one.

The orbital shapes and coupling of spins within the second group of three orbitals in the 'reordered' SC wave function, ψ_4, ψ_3 and ψ_5, closely resemble the SC description of the π space of the allyl radical [76]. The first three orbitals, ψ_2, ψ_6 and ψ_1, are of predominantly σ character but exhibit similar properties. This shows that at the TS the SC active space for the [1,5]-H shift in (*Z*)-1,3-pentadiene involves an allyl-like moiety and its σ-space equivalent. Another example of a SC active space comprised of two allyl-like moieties involving 'antipairs' was observed in the TS for the Cope rearrangement of 1,3,4,6-tetracyano-1,5-hexadiene [77].

The SC wave function at the TS for the [1,5]-H shift in (*Z*)-1,3-pentadiene is very different from two decidedly 'aromatic' SC wave functions, namely those for benzene and for the TS of the Diels–Alder reaction, in both of which the SC orbitals are numbered and ordered in a clockwise fashion around the ring. However, as shown in [57], if the orbitals in benzene are reordered as $\psi_2\psi_6\psi_1\psi_4\psi_3\psi_5$ and the spin-coupling pattern is expressed in the Serber spin basis, the description becomes very similar to that at the TS for the [1,5]-H shift in (*Z*)-1,3-pentadiene. An additional symmetry-constrained SC calculation on benzene produced an 'antipair' solution which is only about one millihartree above the well-known unconstrained solution which is found to possess localised orbitals. The orbitals from the 'antipair' solution are shown in Figure 12 (the orbitals from the standard solution are visually indistinguishable from ψ_1).

As the very small energy gap between the standard and 'antipair' SC solutions for benzene makes the latter a viable alternative description of the molecule, it can be argued that the TS for the [1,5]-H shift in (*Z*)-1,3-pentadiene should be considered to be aromatic. The fact that it is possible to devise a SC wave function for benzene which involves 'antipairs' and that is only 1 millihartree above the well-known standard SC wave function, indicates that the presence of 'antipairs' in a SC description should not be considered, on its own, as a reliable indication of antiaromatic, radical or diradical character.

The SC description of the electronic mechanism of the thermally-allowed suprafacial [1,3] sigmatropic shift linking bicyclo[3.2.0]hept-2-ene and bicyclo[2.2.1]hept-2-ene (norbornene) [58], shown in Scheme H, provided interesting insights into the way in which bonds break and form along the 'suprafacial with inversion' pathway, and revealed

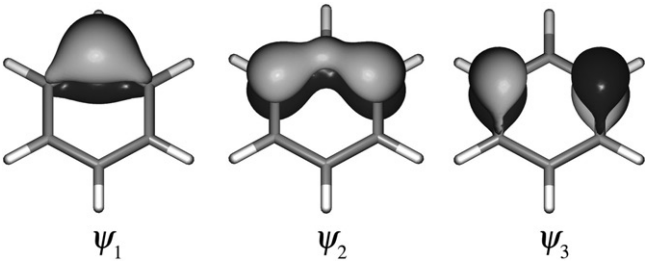

Figure 12. Symmetry-unique SC orbitals from the 'antipair' wave function for benzene.

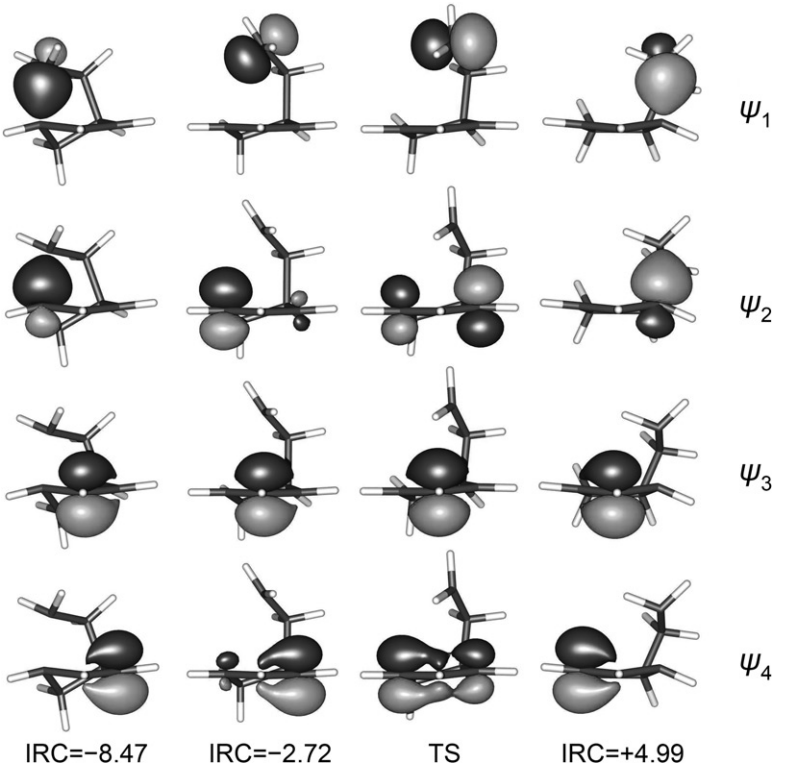

Figure 13. The SC orbitals at various stages of the gas-phase [1,3] sigmatropic rearrangement linking bicyclo[3.2.0]hept-2-ene and bicyclo[2.2.1]hept-2-ene (norbornene). Distances along the IRC in amu$^{1/2}$bohr.

in a very clear way the singlet diradical character of the reacting system in the neighbourhood of the transition state.

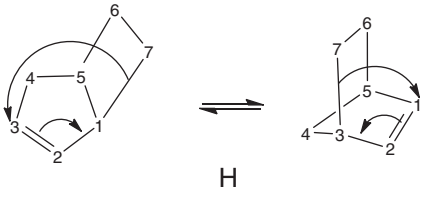

The four active orbitals ψ_1–ψ_4 for the ground state SC(4) wave function are displayed in Figure 13 for four representative geometries along the IRC. At the beginning (rightmost column) and end (leftmost column) of this reaction, each SC orbital is well localised at one carbon atom. Orbitals ψ_1 and ψ_2 resemble two sp^3-like hybrids involved in a σ bond, C_1–C_7 for the reactant and C_3–C_7 for the product. Orbitals ψ_3 and ψ_4 each resemble distorted $2p_\pi$ AOs, with tails in each other's direction, forming the π bond in the reactant (C_2–C_3) and in the product (C_1–C_2). Moving from the reactant geometry towards the transition state, ψ_1 remains well-localised at C_7, but changes its shape to that of a $2p_\pi$ AO whilst turning by about 90° around the C–C bond between C_6 and C_7. Approaching the

product, this orbital rotates further in the same direction and, as shown in Figure 13, it completes a 180° turn (consistent with inversion of the configuration at C_7) so as to become involved in the new σ bond to C_3. During the reaction, ψ_2 shrinks at C_1, where it was located (as an sp^3-like orbital) for the reactant, and it grows at C_3. As can be seen from Figure 13, it actually takes the form at the TS of an antisymmetric combination of two $2p_\pi$ AOs which are semilocalised on two non-neighbouring atomic centres (C_1 and C_3). Nearer the product, ψ_2 evolves into an sp^3-like orbital at C_3. Throughout the reaction, ψ_3 remains localised at C_2, simply changing its direction of distortion from C_3 to C_1. On the other hand, ψ_4 moves between C_3 and C_1, in the direction opposite to that seen for ψ_2. Furthermore, unlike ψ_2, orbital ψ_4 takes the form of a symmetric combination of $2p_\pi$ atomic orbitals on C_1 and C_3 at the transition state, with also some density associated with C_2. Nearer the product, it evolves into a distorted $2p_\pi$-like orbital on C_1.

Throughout the reaction path, the spin-coupling pattern remains dominated by the spin function which couples the spins of the electrons within the orbital pairs (ψ_1,ψ_2) and (ψ_3,ψ_4) to singlets. However, around the TS the orbital overlap $\langle\psi_1|\psi_2\rangle$ drops to rather low values which, in combination with the shapes of these singlet-coupled orbitals (see the TS column in Figure 13), is a clear indication of singlet biradical character.

3.6. *S_N2 identity reactions*

As demonstrated in [54] SC theory can also provide a clear picture of the electronic rearrangements taking place during gas phase S_N2 identity reactions,

$$Cl^- + RCl \rightarrow ClR + Cl^-$$

where R is an alkyl group. As the generally accepted notion is that these reactions involve four active electrons, two from the forming σ bond and two from the breaking σ bond, the SC calculations were performed with a wave function including four active orbitals. For all of the S_N2 identity reactions studied it was observed that these four orbitals are engaged in two pairs, both of which are preserved during the course of the reaction. Initially, one of the orbitals pairs is on the incoming nucleophile and the other one is engaged in the R–Cl bond. At the transition state, the bond-formation and bond-breaking processes are almost equally advanced and the pairs are responsible for the bonding interactions between R and the incoming and leaving nucleophiles (Figure 14). Beyond the transition state, the pair that was initially on the incoming nucleophile becomes engaged in the forming bond, while the other pair localises onto the leaving nucleophile.

It is informative to compare the shapes of the SC orbitals at the transition states of the reactions involving CH_3Cl and Cl^-, CH_3CH_2Cl and Cl^- and $C(CH_3)_3Cl$ and Cl^-. Whereas the transition states for the CH_3Cl and Cl^- and for the CH_3CH_2Cl and Cl^- reactions show well-defined Cl–C–Cl bonding interactions, slightly weakened for the second reaction, the SC model for the TS of the S_N2 gas-phase identity reaction between $C(CH_3)_3Cl$ and Cl^- can be described fairly accurately as involving a $C(CH_3)_3^+$ carbocation 'clamped' between two Cl^- anions. This suggests a tendency for a switch from the S_N2 to the S_N1 mechanism. A mechanism of this type cannot be properly described within a gas-phase study, but it is obvious that in the presence of suitable solvent molecules the components of the TS would separate to form individual solvated $C(CH_3)_3^+$ and Cl^- ions.

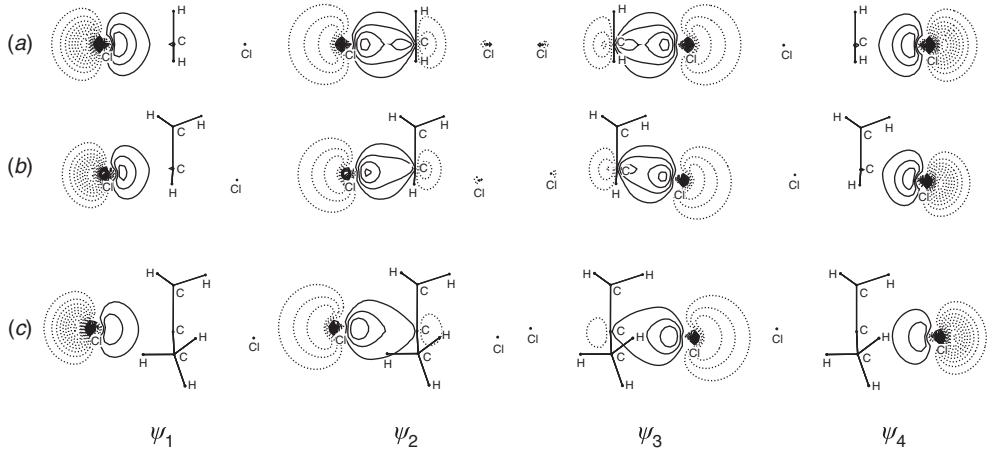

Figure 14. The SC orbitals at the transition states of the S_N2 identity reactions involving (a) CH_3Cl and Cl^-, (b) CH_3CH_2Cl and Cl^- and (c) $C(CH_3)_3Cl$ and Cl^-.

It is also interesting to compare different halogens. The SC descriptions of the $CH_3Cl + Cl^-$ and $CH_3F + F^-$ gas-phase S_N2 identity reactions were found to be qualitatively similar, but a significantly larger extent of bond formation was observed at the TS for the fluorine case, with electronic rearrangements starting within a much earlier region of the reaction path.

3.7. *Future developments*

The last few years have continued to see a rapid increase in the number of applications of CASSCF-based approaches to chemical problems. Typically the numbers of active electrons treated in such studies are such that analogous SC calculations would already be entirely practical using existing codes. On the other hand, not all choices of CASSCF active space are likely to lead to easy-to-interpret SC descriptions that are based on a single orbital product. In general, we are currently interested mostly in choices of active space for which the number of orbitals matches the number of electrons. In some instances, this may require using a larger SC active space than would usually be considered in a CASSCF treatment [42]. Nonetheless, there is certainly a very wide range of interesting problems in organic reactivity to which SC theory could already be applied.

Given that it represents the most general *ansatz* which employs a single orbital product, an important next step could be to make better quantitative use of the SC wave function in subsequent calculations that take proper account of dynamic electron correlation. In contrast to the most popular spin-adapted single orbital product wave function, namely the closed-shell Slater determinant used in RHF theory, the SC wave function, just like its CASSCF counterpart, can usefully be calculated at practically any geometry on the potential energy surface for any reaction as long as the chosen active space is sufficient to describe all bond-breaking and bond-formation processes. This potentially makes the SC wave function a highly appropriate reference for developing higher-level CI, many-body perturbation theory or coupled-cluster (CC) approaches. Several CI and multi-reference

(MR) post-SC methods have already been formulated, including SCVB [38], SCVB* [78–80], MR-SCVB* [80,81] and GMCSC [82,83]. Various multi-reference spin-coupled (MRSC) calculations can also already be carried out using the CASVB module, as incorporated in MOLPRO [29] and in MOLCAS [30]. However, the real challenge is of course to develop SC-based equivalents of size-consistent and size-extensive HF-based approaches such as MP2 and CCD. Additionally, QM/MM approaches in which the QM part includes a SC or MRSC construction could become powerful tools for studying the electronic mechanisms of biologically-important reactions.

4. Conclusions

Spin-coupled theory provides highly visual direct insights into the electronic rearrangements that accompany the bond-breaking and bond-formation processes in organic chemical reactions. Being based on the most general wave function constructed from a single orbital product, it arguably represents the highest level of theory at which one can obtain directly such orbital models of correlated electronic structure. series of SC calculations along the minimum energy paths of a wide range of reactions have provided new, interesting and often unexpected insights into the electronic mechanisms of such reactions. In some cases, the descriptions that can be found in standard organic chemistry textbooks are faithfully reproduced, except for important differences as to the precise meanings of dots and arrows schemes. In other cases, the SC descriptions do not follow traditional expectations but, with hindsight, do make considerable sense. As well as being useful in their own right, such SC descriptions can also provide benchmarks for assessing the veracity of qualitative descriptions extracted less directly by analyzing MO-theory and DFT electron densities.

Note

1. The much read author Lewis Carroll made extensive use of words formed by merging parts of two or more other words. For example, he used 'slithy' to mean 'lithe and slimy', with two meanings packed up in one word (portmanteaux). Remembering that 'CASSCF' is the standard abbreviation for complete active space self-consistent field, and that 'SCVB' has been used as an abbrevation for spin-coupled valence bond, the name 'CASVB' comes about as if you started by saying 'CASSCF' but, part way through, decided that what you had really wanted to say is 'SCVB'. (Other groups have instead adopted the label CASVB as an abbreviation for complete active space valence bond, and have named calculations and codes accordingly.)

References

[1] D. J. Klein and N. Trinajstić (editors), *Valence Bond Theory and Chemical Structure* (Elsevier, Amsterdam, 1990).
[2] D. L. Cooper (editor), *Valence Bond Theory* (Elsevier, Amsterdam, 2002).
[3] R. B. Woodward and R. Hoffmann, Angew. Chem. Int. Ed. Engl. **8**, 781 (1969).
[4] R. B. Woodward and R. Hoffmann, *The Conservation of Orbital Symmetry* (Verlag Chemie, Weinheim, 1970).
[5] K. Fukui, Acc. Chem. Res. **4**, 57 (1971).
[6] M. J. S. Dewar, Tetrahedron Suppl. **8**, s75 (1966).

[7] H. E. Zimmerman, J. Am. Chem. Soc. **88**, 1564 (1966).
[8] H. E. Zimmerman, Acc. Chem. Res. **4**, 272 (1971).
[9] J. Gerratt and W. N. Lipscomb, Proc. Natl. Acad. Sci. (USA) **59**, 332 (1968).
[10] R. C. Ladner and W. A. Goddard III, J. Chem. Phys. **51**, 1073 (1969).
[11] N. C. Pyper and J. Gerratt, Proc. Roy. Soc. Lond. Ser. A **355**, 407 (1977).
[12] D. L. Cooper, J. Gerratt, M. Raimondi, M. Sironi, and T. Thorsteinsson, Theor. Chim. Acta **85**, 261 (1993).
[13] R. McWeeny, Proc. Roy. Soc. Lond. Ser. A **223**, 306 (1954).
[14] P. B. Karadakov, J. Gerratt, D. L. Cooper, and M. Raimondi, J. Chem. Phys. **97**, 7637 (1992).
[15] T. Thorsteinsson, D. L. Cooper, J. Gerratt, P. B. Karadakov, and M. Raimondi, Theor. Chim. Acta **93**, 343 (1996).
[16] T. Thorsteinsson and D. L. Cooper, Theor. Chim. Acta **94**, 233 (1996).
[17] D. L. Cooper, T. Thorsteinsson, and J. Gerratt, Adv. Quant. Chem. **32**, 51 (1998).
[18] T. Thorsteinsson and D. L. Cooper, J. Math. Chem. **23**, 105 (1998).
[19] T. Thorsteinsson and D. L. Cooper, in *Quantum Systems in Chemistry and Physics. Volume 1: Basic Problems and Model Systems*, edited by A. Hernández-Laguna, J. Maruani, R. McWeeny, and S. Wilson (Kluwer, Dordrecht, 2000), p. 303.
[20] G. Rumer, Göttinger Nachr. **3**, 337 (1932).
[21] M. Kotani, A. Amemyia, E. Ishiguro, and T. Kimura, *Tables of Molecular Integrals* (Maruzen, Tokyo, 1963).
[22] R. Serber, Phys. Rev. **45**, 461 (1934).
[23] R. Serber, J. Chem. Phys. **2**, 697 (1934).
[24] P.-O. Löwdin, Phys. Rev. **97**, 1509 (1955).
[25] P.-O. Löwdin, Rev. Mod. Phys. **36**, 966 (1964).
[26] M. Simonetta, E. Gianinetti, and I. Vandoni, J. Chem. Phys. **48**, 1579 (1968).
[27] R. Pauncz, *Spin Eigenfunctions* (Plenum Press, New York, NY, 1979).
[28] P. B. Karadakov, J. Gerratt, D. L. Cooper, and M. Raimondi, Theor. Chim. Acta **90**, 51 (1995).
[29] H.-J. Werner, P. J. Knowles, R. Lindh, F. R. Manby, M. Schütz, P. Celani, T. Korona, A. Mitrushenkov, G. Rauhut, T. B. Adler, R. D. Amos, A. Bernhardsson, A. Berning, D. L. Cooper, M. J. O. Deegan, A. J. Dobbyn, F. Eckert, E. Goll, C. Hampel, G. Hetzer, T. Hrenar, G. Knizia, C. Köppl, Y. Liu, A. W. Lloyd, R. A. Mata, A. J. May, S. J. McNicholas, W. Meyer, M. E. Mura, A. Nicklaß, P. Palmieri, K. Pflüger, R. Pitzer, M. Reiher, U. Schumann, H. Stoll, A. J. Stone, R. Tarroni, T. Thorsteinsson, M. Wang, and A. Wolf, *MOLPRO Version* 2008.1 (Cardiff, UK, 2008).
[30] G. Karlström, R. Lindh, P.-Å. Malmqvist, B. O. Roos, U. Ryde, V. Veryazov, P. O. Widmark, M. Cossi, B. Schimmelpfennig, P. Neogrady, and L. Seijo, MOLCAS: A Program Package for Computational Chemistry, Computational Material Science **28**, 222 (2003).
[31] D. L. Cooper, J. Gerratt, and M. Raimondi, Nature **323**, 699 (1986).
[32] D. L. Cooper, S. C. Wright, J. Gerratt, P. A. Hyams, and M. Raimondi, J. Chem. Soc. Perkin Trans. II, 719 (1989).
[33] D. L. Cooper, J. Gerratt, and M. Raimondi, in *Pauling's Legacy – Modern Modelling of the Chemical Bond*, edited by Z. B. Maksić and W. J. Orville-Thomas (Elsevier, Amsterdam, 1999), Chap. 18.
[34] P. B. Karadakov, D. L. Cooper, and J. Gerratt, J. Am. Chem. Soc. **120**, 3975 (1998).
[35] P. B. Karadakov, J. Gerratt, D. L. Cooper, and M. Raimondi, J. Am. Chem. Soc. **115**, 6863 (1993).
[36] T. Thorsteinsson, D. L. Cooper, J. Gerratt, and M. Raimondi, Theor. Chim. Acta **95**, 131 (1997).
[37] P. B. Karadakov, Ann. Rep. Prog. Chem., Sect. C **94**, 3 (1998).
[38] J. Gerratt and M. Raimondi, Proc. Roy. Soc. Lond., Ser. A **371**, 525 (1980).
[39] E. C. da Silva, J. Gerratt, D. L. Cooper, and M. Raimondi, J. Chem. Phys. **101**, 3866 (1994).

[40] M. Sironi, M. Raimondi, D. L. Cooper, and J. Gerratt, J. Chem. Soc. Faraday Trans. 2 **83**, 1651 (1987).
[41] M. Sironi, D. L. Cooper, J. Gerratt, and M. Raimondi, J. Am. Chem. Soc. **112**, 5054 (1990).
[42] P. B. Karadakov, J. Gerratt, D. L. Cooper, and M. Raimondi, J. Chem. Soc. Faraday Trans. **90**, 1643 (1994).
[43] F. Bernardi, A. Bottoni, P. Celani, M. Olivucci, M. A. Robb, and A. Venturini, Chem. Phys. Lett. **192**, 229 (1992).
[44] M. J. Frisch, G. W. Trucks, H. B. Schlegel, G. E. Scuseria, M. A. Robb, J. R. Cheeseman, J. A. Montgomery Jr, T. Vreven, K. N. Kudin, J. C. Burant, J. M. Millam, S. S. Iyengar, J. Tomasi, V. Barone, B. Mennucci, M. Cossi, G. Scalmani, N. Rega, G. A. Petersson, H. Nakatsuji, M. Hada, M. Ehara, K. Toyota, R. Fukuda, J. Hasegawa, M. Ishida, T. Nakajima, Y. Honda, O. Kitao, H. Nakai, M. Klene, X. Li, J. E. Knox, H. P. Hratchian, J. B. Cross, V. Bakken, C. Adamo, J. Jaramillo, R. Gomperts, R. E. Stratmann, O. Yazyev, A. J. Austin, R. Cammi, C. Pomelli, J. W. Ochterski, P. Y. Ayala, K. Morokuma, G. A. Voth, P. Salvador, J. J. Dannenberg, V. G. Zakrzewski, S. Dapprich, A. D. Daniels, M. C. Strain, O. Farkas, D. K. Malick, A. D. Rabuck, K. Raghavachari, J. B. Foresman, J. V. Ortiz, Q. Cui, A. G. Baboul, S. Clifford, J. Cioslowski, B. B. Stefanov, G. Liu, A. Liashenko, P. Piskorz, I. Komaromi, R. L. Martin, D. J. Fox, T. Keith, M. A. Al-Laham, C. Y. Peng, A. Nanayakkara, M. Challacombe, P. M. W. Gill, B. Johnson, W. Chen, M.W. Wong, C. Gonzales, and J. A. Pople, *Gaussian 03, Revision D.01* (Gaussian, Inc., Wallingford, CT, 2005).
[45] J. J. Blavins, D. L. Cooper, and P. B. Karadakov, J. Phys. Chem. A **109**, 231 (2005).
[46] J. G. Hill, D. L. Cooper, and P. B. Karadakov, J. Phys. Chem. A **112**, 12823 (2008).
[47] J. M. Oliva, J. Gerratt, P. B. Karadakov, and D. L. Cooper, J. Chem. Phys. **107**, 8917 (1997).
[48] P. B. Karadakov, D. L. Cooper, T. Thorsteinsson, and J. Gerratt, in *Quantum Systems in Chemistry and Physics. Volume 1: Basic Problems and Model Systems*, edited by A. Hernández-Laguna, J. Maruani, R. McWeeny, and S. Wilson (Kluwer, Dordrecht, 2000), pp. 327–344.
[49] P. B. Karadakov, D. L. Cooper, and J. Gerratt, Theor. Chem. Acc. **100**, 222 (1998).
[50] P. B. Karadakov and D. L. Cooper, J. Phys. Chem. A **105**, 10946 (2001).
[51] J. J. Blavins, P. B. Karadakov, and D. L. Cooper, J. Org. Chem. **66**, 4285 (2001).
[52] J. J. Blavins, P. B. Karadakov, and D. L. Cooper, J. Phys. Chem. A **107**, 2548 (2003).
[53] T. Thorsteinsson, A. Famulari, and M. Raimondi, Int. J. Quantum Chem. **74**, 231 (1999).
[54] J. J. Blavins, D. L. Cooper, and P. B. Karadakov, J. Phys. Chem. A **108**, 914 (2004).
[55] J. J. Blavins, D. L. Cooper, and P. B. Karadakov, Int. J. Quantum Chem. **98**, 465 (2004).
[56] J. G. Hill, P. B. Karadakov, and D. L. Cooper, Theor. Chem. Acc. **115**, 212 (2006).
[57] J. G. Hill, P. B. Karadakov, and D. L. Cooper, Faraday Discuss. **135**, 285 (2007).
[58] P. B. Karadakov, D. L. Cooper, and A. Uhe, Int. J. Quantum Chem. **109**, 1807 (2009).
[59] J. Gerratt, Chem. Br. **23**, 327 (1987).
[60] S. C. Wright, D. L. Cooper, J. Gerratt, and M. Raimondi, J. Phys. Chem. **96**, 7943 (1992).
[61] P. B. Karadakov, J. Gerratt, D. L. Cooper, and M. Raimondi, J. Phys. Chem. **99**, 10186 (1995).
[62] G. Leroy, M. Sana, L. A. Burke, and M. T. Nguyen, in *Quantum Theory of Chemical Reactions*, edited by R. Daudel, A. Pullman, L. Salem, and A. Veillard (D. Reidel, The Netherlands, 1979), Vol. 1, p. 91.
[63] M. Sana, G. Leroy, G. Dive, and M. T. Nguyen, J. Mol. Struct. (THEOCHEM) **89**, 147 (1982).
[64] G. Leroy and M. Sana, Tetrahedron **31**, 2091 (1975).
[65] G. Leroy and M. Sana, Tetrahedron **32**, 709 (1976).
[66] M. T. Nguyen, A. K. Chandra, S. Sakai, and K. Morokuma, J. Org. Chem. **64**, 65 (1999).
[67] R. D. Harcourt, J. Mol. Struct. **12**, 351 (1972).
[68] R. D. Harcourt, J. Phys. Chem. A **105**, 10947 (2001).
[69] R. D. Harcourt and A. Schulz, J. Phys. Chem. A **104**, 6510 (2000).
[70] K. Sakata, J. Phys. Chem. A **104**, 10001 (2000).

[71] M. T. Nguyen, A. K. Chandra, T. Uchimaru, and S. Sakai, J. Phys. Chem. A **105**, 10943 (2001).
[72] D. L. Cooper, J. Gerratt, M. Raimondi, and S. C. Wright, J. Chem. Soc. Perkin Trans. II, 1187 (1989).
[73] D. L. Cooper, J. Gerratt, and M. Raimondi, in *Pauling's Legacy – Modern Modelling of the Chemical Bond*, edited by Z. B. Maksić and W. J. Orville-Thomas (Elsevier, Amsterdam, 1999).
[74] H. Jiao and P. v. R. Schleyer, J. Chem. Soc. Faraday Symp. **90**, 1559 (1994).
[75] H. Jiao and P. v. R. Schleyer, J. Phys. Org. Chem. **11**, 655 (1998).
[76] P. B. Karadakov, J. Gerratt, G. Raos, D. L. Cooper, and M. Raimondi, J. Am. Chem. Soc. **116**, 2075 (1994).
[77] J. J. Blavins, D. L. Cooper, and P. B. Karadakov, J. Phys. Chem. A **108**, 194 (2004).
[78] M. Raimondi, M. Sironi, J. Gerratt, and D. L. Cooper, Int. J. Quantum Chem. **60**, 225 (1996).
[79] N. J. Clarke, M. Raimondi, M. Sironi, J. Gerratt, and D. L. Cooper, Theor. Chem. Acc. **99**, 8 (1996).
[80] M. Sironi, M. Raimondi, R. Martinazzo, F. A. Gianturco, and D. L. Cooper, in *Valence Bond Theory*, edited by D. L. Cooper (Elsevier, Amsterdam, 2002), pp. 261–277.
[81] R. Martinazzo, A. Famulari, M. Raimondi, E. Bodo, and F. A. Gianturco, J. Chem. Phys. **115**, 2917 (2001).
[82] F. E. Penotti, Int. J. Quantum Chem. **59**, 349 (1996).
[83] F. E. Penotti, in *Valence Bond Theory*, edited by D. L. Cooper (Elsevier, Amsterdam, 2002), pp. 279–312.